# IL-13Rα1 Suppresses Tumor Progression in Two-Stage Skin Carcinogenesis Model by Regulating Regulatory T Cells

JIDOpen

Tanja Salomaa[1,2,5], Toini Pemmari[1,5], Juuso Määttä[1,5], Laura Kummola[1,2], Niklas Salonen[1], Martín González-Rodríguez[1], Liisa Parviainen[1,3], Lotta Hiihtola[1], Maria Vähätupa[1], Tero A.H. Järvinen[1,4,5] and Ilkka S. Junttila[1,2,5]

Type 2 inflammation–related cytokine IL-13 plays a protective role in experimental papilloma induction in mice. To understand the mechanisms by which IL-13 contributes to papilloma formation, we utilized *Il13rα1*-knockout (KO) mice in a widely used 7,12-dimethylbenz[*a*]anthracene/12-*O*-tetradecanoyl phorbol-13-acetate two-stage skin carcinogenesis protocol that mimics the development of squamous cell carcinoma. KO mice developed more papillomas and significantly faster than wild-type mice. Papilloma development reduced regulatory T cells in wild-type mice but substantially less in KO mice. In line with this, IL-2 and IL-10 levels decreased in wild-type mice but not in KO mice. Furthermore, systemic IL-5 and TSLP levels were elevated, whereas IL-22 was decreased during papilloma formation in the skin of KO mice. Polymorphonuclear myeloid–derived suppressor cells were decreased in the KO mice at the early phase of papilloma induction. We show that IL-13Rα1 protects from papilloma development in chemically induced skin carcinogenesis, and our results provide further insights into the protective role of functional IL-4 and IL-13 signaling through type II IL-4 receptor in tumor development.

*Journal of Investigative Dermatology* (2021) ■, ■–■; doi:10.1016/j.jid.2021.11.013

## INTRODUCTION

Cancer formation and progression are a result of uncontrolled cell growth. The immune system can recognize malignant cells and control tumor growth by the process of immunoediting. Initially, the immune system aims at eliminating the malignant cells; this step utilizes at least NK cells, CD4/CD8 cells, NKT cells, γδ T cells, macrophages, and dendritic cells (Gonzalez et al., 2018; Hiam-Galvez et al., 2021). Failure to achieve tumor elimination or dormancy will lead to tumor progression (Dunn et al., 2004; Mittal et al., 2014). Suppressive immune cells, such as tumor-associated macrophages (TAMs), regulatory T cells (Tregs), and myeloid-derived suppressor cells (MDSCs), attenuate the immune response against malignant cells (Hiam-Galvez et al., 2021). Humoral inflammation mediators, such as cytokines and chemokines, play a critical role in the development and function of Tregs, TAMs, and MDSCs (Li et al., 2020).

IL-13 is a signature cytokine of type 2 immune response. In type 2 inflammation, the importance of IL-13 was initially shown in mucus production and airway hyperreactivity in lung inflammation (Wills-Karp et al., 1998). IL-13 is also a key mediator of tissue fibrosis and regulates both transforming growth factor β–dependent and –independent fibrosis (Henderson et al., 2020; Kaviratne et al., 2004; Lee et al., 2001). As indicated by knockout (KO) studies, IL-13 plays a protective role in 7,12-dimethylbenz[*a*]anthracene (DMBA)/12-*O*-tetradecanoyl phorbol-13-acetate (TPA)-induced skin carcinogenesis (Rothe et al., 2013). IL-13 also plays a role in the expansion of MDSCs in models of fibrosarcoma, lymphoma, and colon carcinoma (Gabrilovich and Nagaraj, 2009).

IL-13 acts on cells through type 2 IL-4 receptor, consisting of IL-13Rα1 and IL-4Rα. IL-4 can also utilize this same receptor complex (LaPorte et al., 2008). IL-13 has another cell surface receptor, IL-13Rα2, that binds the cytokine with high affinity and is an important inducer of transforming growth factor β expression in macrophages on sustained inflammation (Fichtner-Feigl et al., 2006). Anatomically, of the three receptors regulating IL-13 signaling, IL-4Rα is ubiquitously expressed, IL-13Rα1 is widely expressed outside lymphocytes, and IL-13Rα2 expression is scarce. The expression pattern of the receptors renders IL-13 mainly an effector cytokine (Junttila et al., 2008). In type 2 inflammation, *Il-4* and *Il-4rα* deficiency results in weak CD4 T cell–T helper 2 responses, whereas *Il-13rα1*-KO mice paradoxically have exacerbated CD4 T cell–T helper 2 responses but reduced airway hyperreactivity and mucus production (Ramalingam et al., 2008).

DMBA/TPA two-stage skin carcinogenesis model is one of the most widely used cancer models. We chose to use DMBA/TPA

[1]*Faculty of Medicine and Health Technology, Tampere University, Tampere, Finland;* [2]*Fimlab Laboratories, Tampere, Finland;* [3]*Medfiles Ltd, Kuopio, Finland; and* [4]*Department of Orthopedics & Traumatology, Tampere University Hospital, Tampere, Finland*

[5]*These authors contributed equally to this work.*

*Correspondence: Ilkka S. Junttila, Cytokine Biology Research Group, Faculty of Medicine and Health Technology, Tampere University, Arvo Ylpön katu 34, 33250 Tampere, Finland. E-mail: ilkka.junttila@tuni.fi*

*Abbreviations:* DMBA, 7,12-dimethylbenz[a]anthracene; KO, knockout; LN, lymph node; MDSC, myeloid-derived suppressor cell; TAM, tumor-associated macrophage; TPA, 12-O-tetradecanoyl phorbol-13-acetate; Treg, regulatory T cell; WT, wild-type

*Received 24 June 2021; revised 5 November 2021; accepted 9 November 2021; accepted manuscript published online XXX; corrected proof published online XXX*

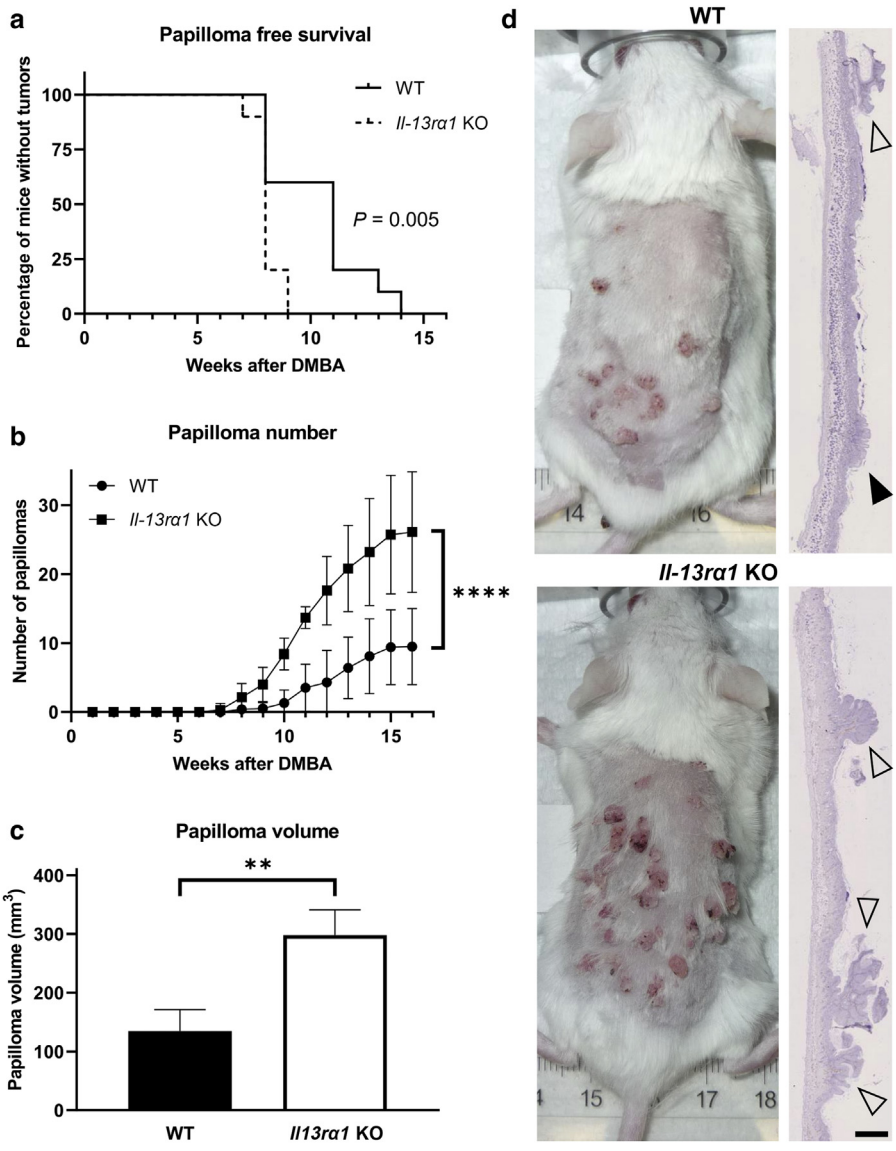


**Figure 1. The deletion of *Il-13rα1* accelerates skin tumor formation.** *Il-13rα1*–deficient mice and WT counterparts were subjected to DMBA/TPA-induced skin carcinogenesis. **(a)** Percentage of WT (solid line) or KO (dashed line) mice without tumors. Data was analyzed with log-rank (Mantel–Cox) test, $P > 0.005$, n = 10 for groups. **(b)** The number of papillomas in WT (circles) and KO (squares) mice at each timepoint, expressed with mean ± SD. Data were analyzed with nonlinear regression, $^{***}P < 0.0001$, n = 10 for groups. **(c)** The total volume of papillomas per one mouse. Data were analyzed with Student's *t*-test, $^{**}P < 0.01$, n = 10 for both groups. **(d)** Representative images of mouse back and hematoxylin-stained histologic skin section at week 16. Macroscopic (open triangles) and microscopic (black triangle) papillomas are indicated. Bar = 1 mm. DMBA, 7,12-dimethylbenz[a] anthracene; KO, knockout; TPA, 12-O-tetradecanoyl phorbol-13-acetate; WT, wild-type.

model, an established experimental model of squamous cell carcinoma (Abel et al., 2009), because, to our knowledge, lack of *Il-13rα1* has not been directly studied in the model, whereas the role of both IL-4 and IL-13 has been studied in mice lacking *Il-4*, *Il-4rα*, or *Il-13*. These studies would suggest a protective role for *Il-13rα1*, albeit not directly studying it (Dalessandri et al., 2016; Rothe et al., 2013). Overall, the studies addressing IL-13 biology by IL-13 cytokine deletion are hampered by the fact that IL-4 may utilize type II IL-4 receptor and compensate for the lack of IL-13. We subjected *Il-13rα1*-KO and wild-type (WT) mice to a two-stage skin carcinogenesis model. Our results suggest that functional IL-4/IL-13 signaling through IL-13Rα1 regulates Tregs and protects against papilloma progression.

## RESULTS

### IL-13Rα1 attenuates tumor development in the skin

We treated the back skin of adult mice deficient for *Il-13rα1* (designed KO) and their respective WT controls once with a local application of the mutagen DMBA and then with the growth-promoting agent TPA twice weekly for a period of 15 weeks. This two-stage skin carcinogenesis treatment induces papillomas derived from the epithelial stem cells and, in particular, from hair follicle stem cells (Li et al., 2013).

The deletion of *Il-13rα1* resulted in the development of papillomas faster than in the WT mice ($P < 0.005$, Figure 1a). The first papillomas were observed in the KO and WT mice 7 and 8 weeks, respectively, after the beginning of the DMBA/TPA treatment, and after 9 weeks, all KO mice had developed papillomas on their back skin, whereas it took 14 weeks for all WT mice to develop papillomas. Furthermore, the KO mice also developed significantly more tumors than the WT mice ($P < 0.0001$, Figure 1b and d). At week 16, the KO mice had developed on average 26 papillomas per mouse, whereas the WT controls had <10 papillomas. Owing to higher papilloma numbers, papilloma burden per mouse was significantly higher in the KO mice as measured by papilloma volume per mouse (WT 134.7 $mm^3$ vs. KO 298.1 $mm^3$, Figure 1c). The proportion of small (<2 mm) and large (>2 mm) papillomas was similar in the KO and WT mice (Supplementary Figure S1a), and accordingly, the volumes of

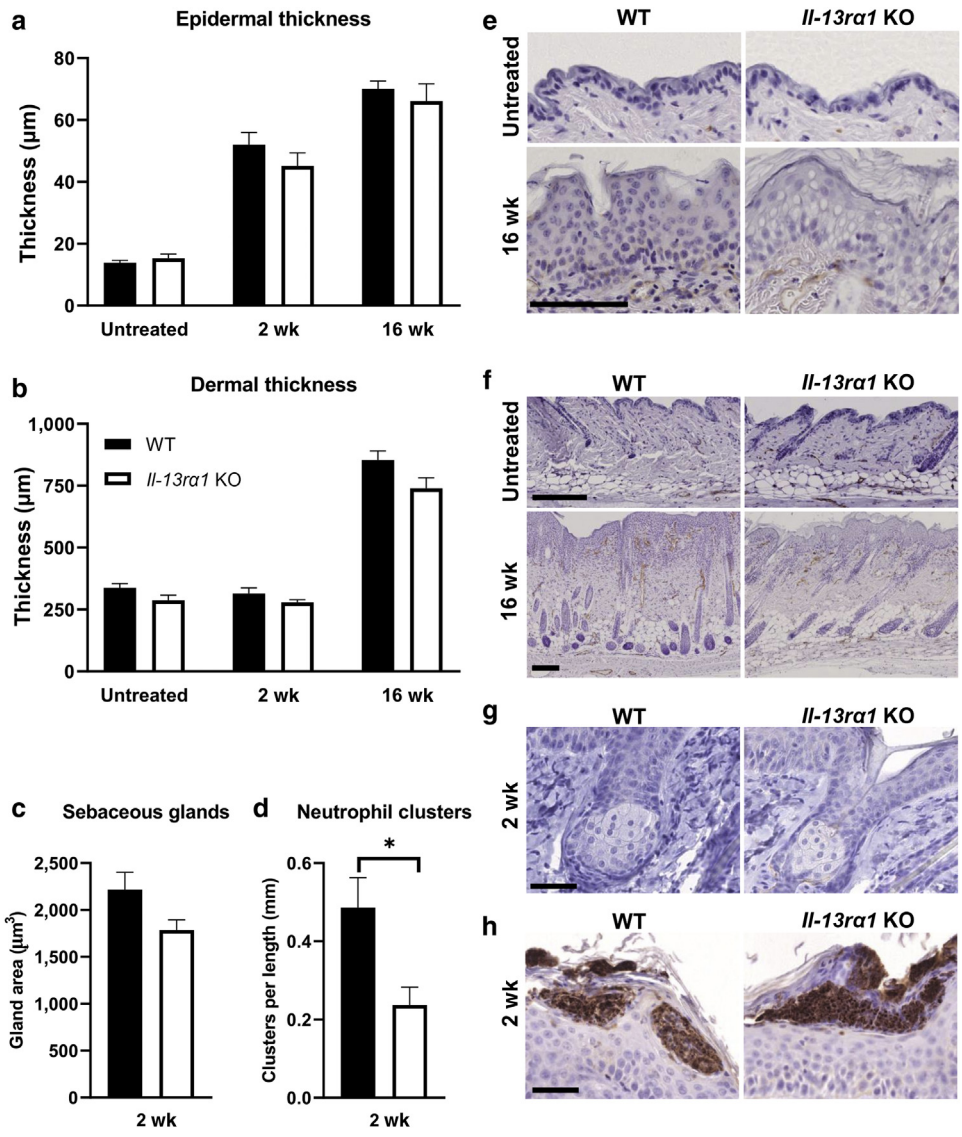


**Figure 2. Skin barrier is not compromised in DMBA/TPA-treated *Il-13rα1*–KO mice.** CD31 stainings were performed in untreated mice or after 2 or 16 weeks of DMBA/TPA treatment. The thickness of the **(a)** epidermis and **(b)** dermis of WT and KO mice with ±SD. Data were analyzed with Student's *t*-test, $*P < 0.05$, n = 6 for untreated and 10 for other groups. **(c)** Sebaceous gland area or **(d)** neutrophil clusters of WT (solid bar) and KO (open bar) mice after 2 weeks of DMBA/TPA treatment. Data were analyzed with Student's *t*-test, $*P < 0.05$. Histologic images of the epidermis in untreated mice and after 16 weeks of DMBA/TPA treatment. Staining was done with CD31 antibody and hematoxylin. Bar = 100 μm in **e** or 200 μm in **f**. Representative histology of **(g)** sebaceous glands and **(h)** neutrophil clusters after 2 weeks of DMBA/TPA treatment. Staining was done with hematoxylin or neutrophil elastase and hematoxylin. Bar = 50 μm. DMBA, 7,12-dimethylbenz[a] anthracene; KO, knockout; TPA, 12-O-tetradecanoyl phorbol-13-acetate; wk, week; WT, wild-type.

individual papillomas from WT or KO mice were similar (Supplementary Figure S1b).

**Cell proliferation, angiogenesis, and immune cell infiltration during papilloma formation in WT and KO mice**

To understand the mechanism of the skin tumor–inhibiting function of IL-13Rα1, we performed an additional short, 2-week treatment of the back skin by the local application DMBA and then with the TPA twice within a week. No significant difference in the thickness of the epidermis or dermis was observed between the KO and WT mice in the untreated group or in either of the two time points (Figure 2a, b, e, and f). In this work, the untreated group refers to steady-state mice at the onset of DMBA/TPA treatment because our emphasis was on understanding the role *Il-13rα1* deletion plays in active tumor formation and progression. Thus, we wanted to exclude the possibility that intrinsic differences between the mice lines existed already at the onset of the experiment. Sebaceous glands' surface area as a read out for sebum expression was similar between WT and KO mice (Figure 2c and g). We determined skin barrier function by measuring the density of neutrophil clusters along dermal–epidermal junction and showed enhanced (by that measure) barrier function in the KO mice (Figure 2d and h). mRNA of antimicrobial peptides *Camp, Defb4,* and *Lcn2* were similarly expressed in the WT and KO skin (Supplementary Figure S2).

WT and KO mice had no difference in cell proliferation rates (Ki-67) in the epidermis or dermis of the untreated and DMBA/TPA-treated skin (Supplementary Figure S3a, b, and e). Interestingly, the epidermal Ki-67 staining pattern at the 2-week time point appeared thinner in the KO mice (Supplementary Figure S3e). We thus analyzed the thickness of proliferating cell area in the epidermis and its relative ratio to epidermal thickness (Supplementary Figure S3c and d). There was a small reduction (albeit statistically significant) in the relative thickness of proliferating cell layer. Proliferation rates were identical in hair bulge and sebaceous glands (Supplementary Figure S3f).

In the DMBA/TPA model, tumor angiogenesis manifests first by increased blood vessel density and later, during

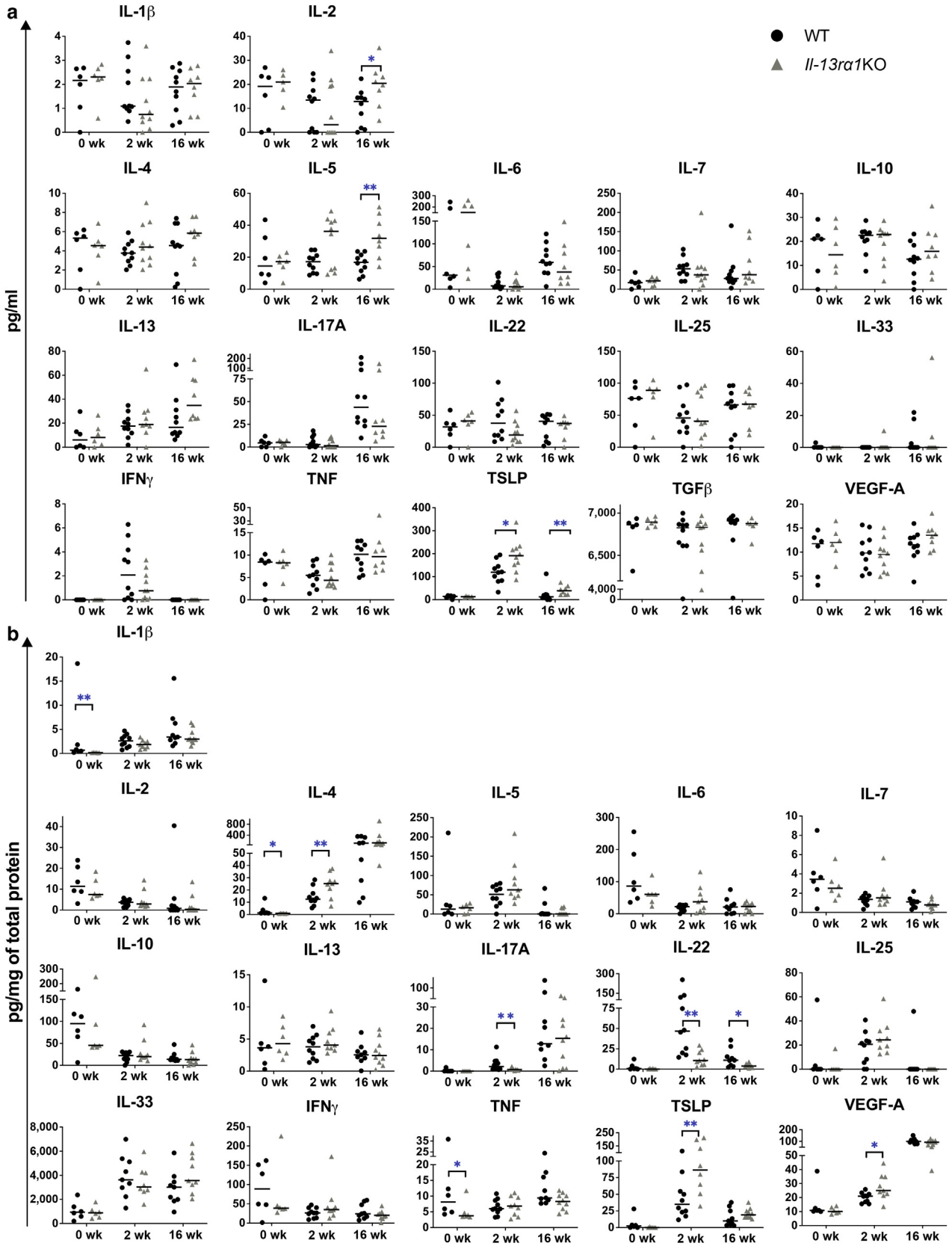


**Figure 3. Systemic (serum) and local (skin) cytokine production in *Il-13rα1*–KO and WT mice in DMBA/TPA-induced skin carcinogenesis model.** The experiment was performed as detailed in Figure 1. At wks 0 (untreated), 2, or 16 after DMBA/TPA treatment, mice were killed. Cytokine levels were measured from **(a)** serum or from **(b)** skin homogenate lysates. Each symbol represents an individual mouse; lines indicate the median. The data were analyzed with Mann–Whitney U test, $*P < 0.05$, $**P < 0.01$, $***P < 0.001$. Group sizes in serum: untreated: n = 6 per strain, at wk 2: n = 10 per strain, and at wk 16: n = 10 for WT and n = 8 for KO strains. Group sizes in skin: untreated: n = 6 per strain, at wk 2: n = 10 for WT and n = 9 for KO strains, and at wk 16: n = 9 for WT and n = 10 for KO strains. DMBA, 7,12-dimethylbenz[a]anthracene; KO, knockout; TPA, 12-O-tetradecanoyl phorbol-13-acetate; wk, week; WT, wild-type.

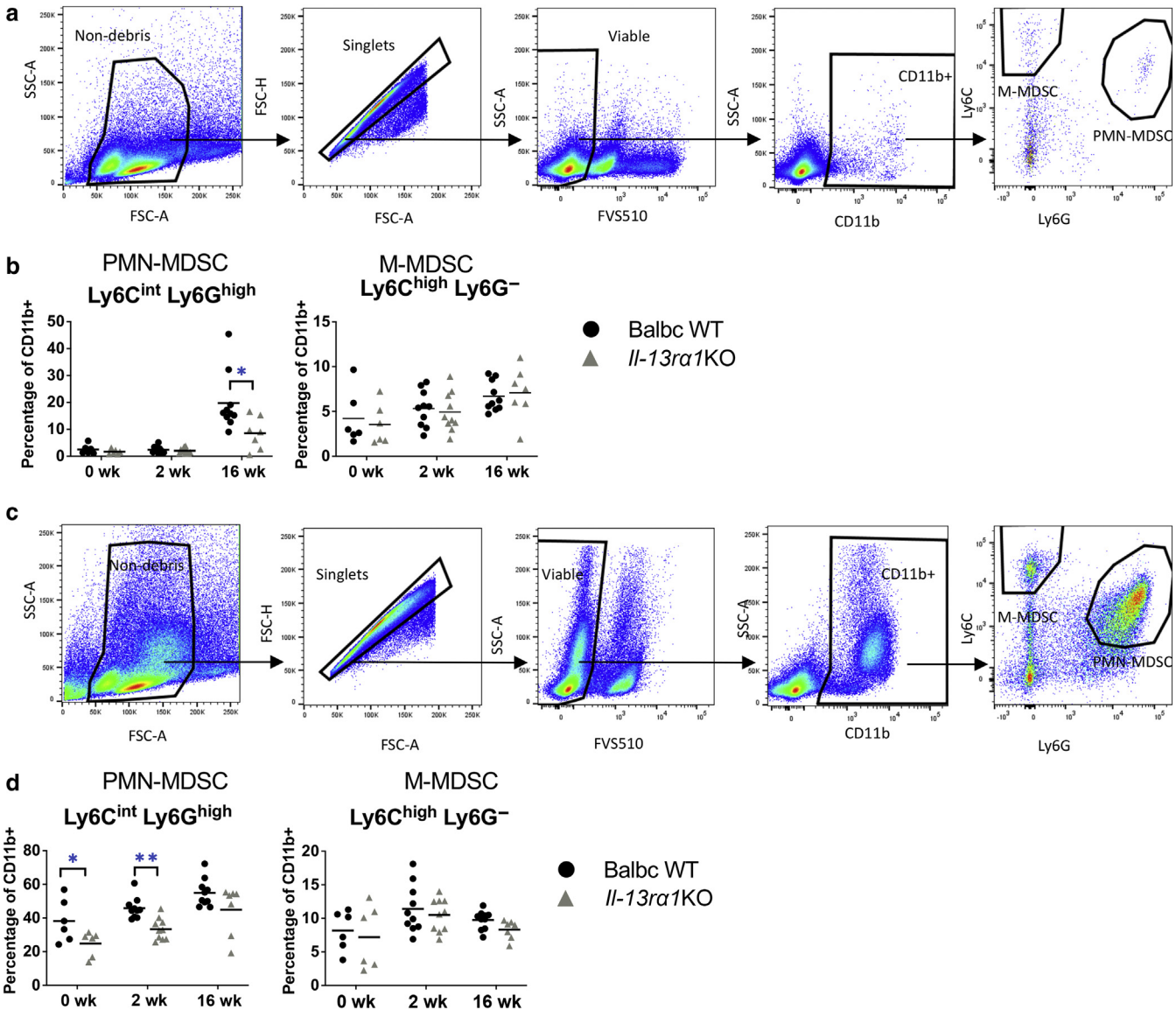


**Figure 4. MDSCs in lymph nodes and spleen during DMBA/TPA-induced skin carcinogenesis model.** At wks 0 (untreated), 2, and 16 of DMBA/TPA treatment, mice were killed, and spleen and skin draining lymph nodes were harvested. **(a)** Flow cytometric gating and representative figure of MDSCs in the lymph nodes at wk 16. **(b)** Percentages of $Ly6C^{int}Ly6G^{high}$ or $Ly6C^{hi}Ly6G-$ cells of all $CD11b^{+}$ cells in the lymph nodes. **(c)** Gating and representative figure of MDSCs in the spleen at wk 16. **(d)** Percentages of $Ly6C^{int}Ly6G^{high}$ and $Ly6C^{hi}Ly6G-$ cells of all CD11b+ cells in the spleen. Each symbol represents an individual mouse; lines indicate the mean. Data were analyzed using Student's *t*-test, $*P < 0.05$, $**P < 0.01$, $***P < 0.001$. Group sizes: untreated: n = 6 both strains, at wk 2: n = 10 for WT, n = 9 for KO, and at wk 16: n = 10 for WT, n = 7 for KO. DMBA, 7,12-dimethylbenz[a]anthracene; FSC, forward scatter; KO, knockout; M-MDSC, monocytic myeloid-derived suppressor cell; PMN-MDSC, polymorphonuclear myeloid-derived suppressor cell; SSC, side scatter; TPA, 12-*O*-tetradecanoyl phorbol-13-acetate; wk, week; WT, wild-type.

papilloma formation, by increased blood vessel lumen (Bolontrade et al., 1998; D'Amico et al., 2020; De Rossi et al., 2021). Similar blood vessel densities were identified in WT and KO mice throughout the experiment (Supplementary Figure S4c), but the blood vessel lumens were significantly larger in WT than in KO mice in DMBA/TPA-treated skin as well in the papillomas (Supplementary Figure S4a and b). We also studied whether the inflammatory cell infiltration in response to DMBA/TPA could be affected in mice lacking *Il-13rα1*. For this, we quantified skin $CD3^{+}$ T cells, macrophages (F4/80+), NK cells ($CD49b^{+}$), and neutrophils (elastase) from the histologic sections. All the four inflammatory cell populations were similar after 16 weeks of DMBA/TPA treatment (Supplementary Figures S5 and S6). We did observe increased CD3 cells in the epidermis of the KO mice at a 2-week time point. Further analysis of T cells showed that CD8 T cells at least partially could explain this increase (Supplementary Figure S7a and c). CD8 T cells can be recruited to tumors by CXCL16—CXCR6 interaction (Di Pilato et al., 2021). We found induction of several components of this pathway in the skin, but no difference between WT and KO at a 2-week time point (Supplementary Figure S8a). Tregs appeared to be slightly elevated in the epidermis of the KO mice, but this trend was not statistically significant (Supplementary Figure S7b and c). We also calculated CD3-, CD8-, and FOXP3-positive hair

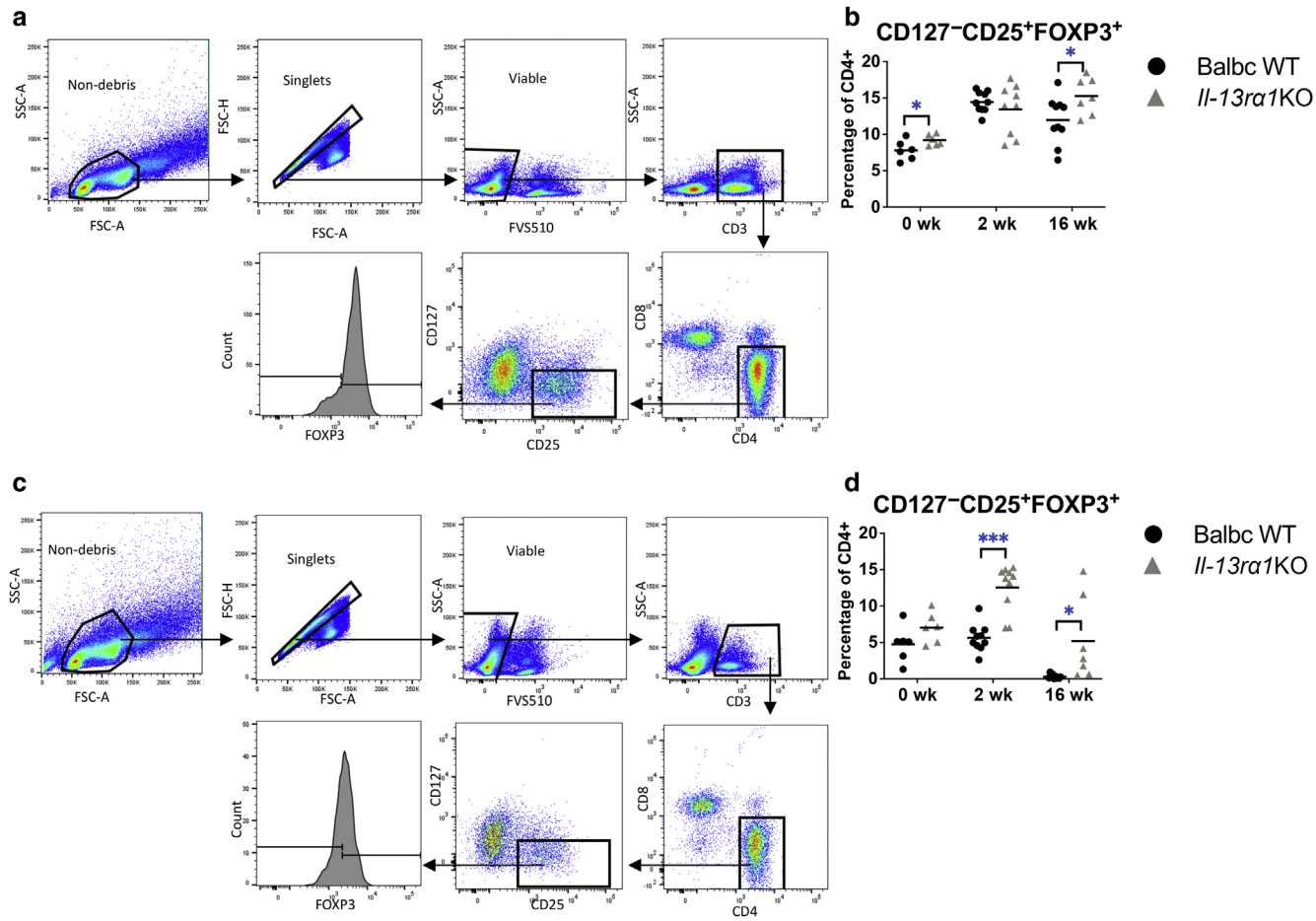


**Figure 5. Number of Tregs in lymph nodes and spleen during papilloma formation.** The experiment was performed as detailed in Figure 1. **(a)** Flow cytometric gating strategy and representative figure of Tregs in the lymph nodes at week 16. FOXP3+ gate was set with non–T cells. **(b)** Percentages of Tregs (CD127-CD25+FOXP3+ of CD4+ cells) in the lymph nodes. **(c)** Gating strategy and representative figure of Tregs in the spleen at week 16. FOXP3+ gate was set with non–T cells. **(d)** Percentages of Tregs (CD127-CD25+FOXP3+ of CD4+ cells) in the spleen. In graphs, each symbol represents an individual mouse; lines indicate the mean. The data were analyzed with Student's *t*-test, $*P < 0.05$, $**P < 0.01$, $***P < 0.001$. Group sizes: untreated: n = 6 both strains, at wk 2: n = 10 for WT, n = 9 for KO, and at wk 16: n = 10 for WT, n = 7. FSC, forward scatter; KO, knockout; SSC, side scatter; Treg, regulatory T cell; wk, week; WT, wild-type.

bulges; the KO mice had fewer FOXP3-negative hair bulges (Supplementary Figure S7d). Treg-specific chemokine or chemokine receptors (Barsheshet et al., 2017) were not differentially expressed in WT or KO skin (qPCR) (Supplementary Figure S8b).

### IL-2, IL-5, IL-22, and TSLP cytokines are induced in mice lacking *Il-13rα1*

Next, we measured cytokine levels from serum (Figure 3a and Supplementary S9a) and skin (Figure 3b and Supplementary Figure S9b). Only significant differences between WT and KO mice are indicated in Figure 3 (*P*-values within WT or KO groups are shown in Supplementary Table S1).

IL-2, IL-5, and TSLP were elevated more in the serum of KO mice than in that of WT mice at week 16 (IL-2 $P < 0.034$, IL-5 $P < 0.004$, TSLP $P < 0.009$). On week 2, only TSLP expression was significantly different ($P < 0.011$) between the two mice lines. Interestingly, the expression of immunosuppressive IL-10 was decreased between weeks 2 and 16 but only in WT mice (week 2 vs. 16: $P < 0.005$).

Cytokine expression in the skin and tumors indicated that at a 2-week time point, differences were observed in the expression of IL-4, IL-17A, IL-22, TSLP, and VEGF-A, (respective *P*-values: $P < 0.0015$, $P < 0.003$, $P < 0.001$, $P < 0.003$, $P < 0.0016$, and $P < 0.022$). By week 16, only IL-22 and IL-27 were different between the mice (respective *P*-values: $P < 0.022$ and $P < 0.043$).

### The number of Ly6C$^{int}$Ly6G$^{hi}$ MDSCs is reduced in KO mice

Because *Il-13rα1* expression is mainly a feature of myeloid and nonhematopoietic cells (Junttila et al., 2008), we studied whether MDSCs (Veglia et al., 2018) or TAMs (Jeannin et al., 2018) are affected by the deletion of *Il-13rα1* in DMBA–TPA model. MDSC subtypes were characterized on the basis of their different expression profiles of Ly6C, Ly6G, F4/80, CD11c, and major histocompatibility complex II surface markers (Veglia et al., 2018). We identified TAMs as CD11b+, F4/80+, major histocompatibility complex II low, CD115+, and Ly6C$^{low/int}$Ly6G- cells (MDSC gating strategies for lymph node (LN) and spleen are in Figure 4, and TAM gating strategy is in Supplementary Figure S10a).

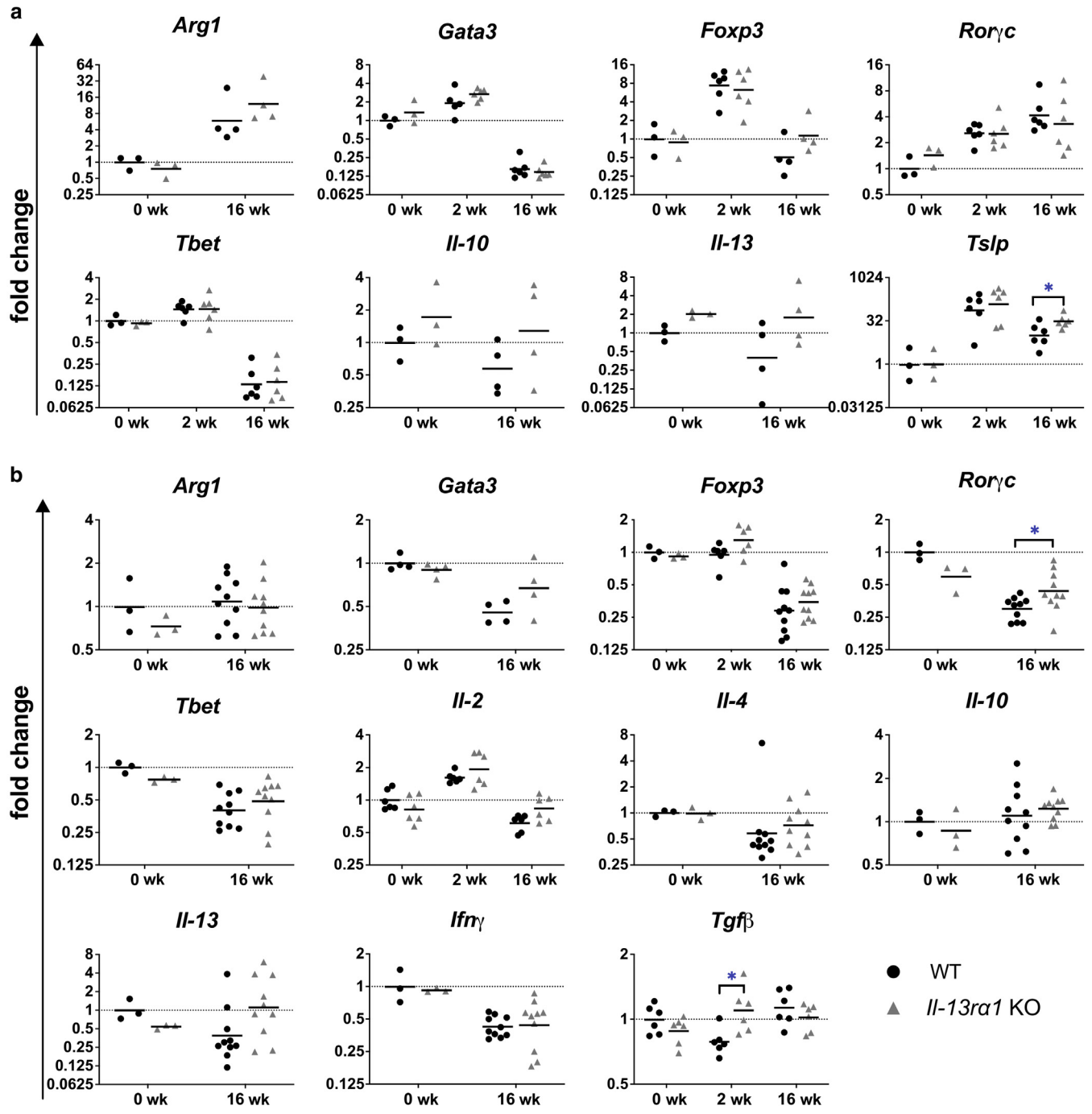


**Figure 6. qPCR analysis of the gene expression of cytokines and transcription factors in the skin and spleen during papilloma formation.** The experiment was performed as detailed in Figure 1. Mice were killed, and spleen and skin were harvested. qPCR analysis for various genes was performed from the **(a)** skin or **(b)** spleen. DeltadeltaCt method was used, and graphs represent fold changes ($2^{-\Delta\Delta Ct}$ method) in (two-fold) logarithmic Y-axis. Each symbol represents an individual mouse (mean of three technical replicates per mouse); lines indicate geometric mean. Data were analyzed with Mann–Whitney *U* test, **P.* <0.05, ***P* < 0.01, ****P* < 0.001. KO, knockout; wk, week; WT, wild-type.

There was a clear difference in the percentage of polymorphonuclear MDSCs between WT and KO mice: KO mice had fewer polymorphonuclear MDSCs in both LN and spleen. The difference was significant in LN after 16 weeks ($P < 0.0264$) and in the spleen in untreated mice and after 2-week treatment ($P < 0.0496$ and $P < 0.0004$, respectively). For the monocytic MDSCs or TAM compartments, we found no differences between WT and KO mice (Figure 4b and d and Supplementary Figure S10b).

### Tregs are elevated in KO mice

Murine lymphocytes express few or no *Il-13rα1* (Andrews et al., 2002) and thus would not be expected to be directly regulated by IL-13. Because Tregs are a key mechanism by which the immune system balances peripheral tolerance and efficient immune defense (Akkaya and Shevach, 2020), we next explored the possibility that IL-4/IL-13 signaling through type 2 IL-4 receptor might regulate the number of Tregs during papilloma formation. A clear increase in the amount

of Tregs was observed in the LN of KO mice after treatment with DMBA/TPA (Figure 5b). Despite the increase being evident in both WT and KO mice, Tregs were consistently higher in KO mice than in the WT, both in normal mice and at the end of the carcinogenesis experiment ($P < 0.0496$ and $P < 0.0383$, respectively).

Splenic Tregs were completely abolished in the WT mice after 16 weeks of treatment (Figure 5d). Tregs seem to decrease also in KO mice, but the KO mice exhibit more Tregs in all the three treatment groups; the difference was significant for 2 and 16 weeks of treatment, respectively ($P < 0.0001$ and $P < 0.0149$). Collectively, Tregs increased in the LNs and decreased in the spleen during the DMBA/TPA treatment. There are more splenic and LN Tregs in KO mice than in WT.

### Expression of immune response–related genes in the skin and spleen during DMBA/TPA treatment

To further characterize the immune landscape, we measured the mRNA expression levels of *Foxp3*, *Tbet*, *Gata3*, *Rorγ*, *Arg1*, *Tslp*, *Il-10*, and *Il-13* from the skin (weeks 0 and 2) and directly from papillomas (biopsies, week 16), as indicated (Figure 6a) (the significant *P*-values over time points are in Supplementary Table S2, and the primer sequences are in Supplementary Table S3). We found that *Arg1* expression was elevated during papilloma formation both in WT and KO mice, indicating that type 1 IL-4 receptor is critical for *Arg1* expression in macrophages (Ramalingam et al., 2008). CD4 T-cell lineage–specific transcription factors were identical between WT and KO at all time points. Whereas *Il-10*, *Foxp3*, and *Il-13* levels were similar between WT and KO mice on week 16, *Tslp* mRNA expression was significantly higher in KO than in the WT mice (Figure 6a). *Il-13rα1* was downregulated in papillomas at 16 weeks ($P < 0.01$), whereas modest changes in the expression of *Il-13rα2* were observed in the papillomas (Supplementary Figure S11a). Components of TSLP receptor were identical between WT and KO mice, indicating that TSLP does not induce the expression of its receptor chain components (Supplementary Figure S11a).

The expression of *Arg1*, *Il-10*, *Il-13*, *Ifnγ*, *Tbet*, *Tgfb*, *Gata3*, *Il-4*, and *Foxp3* was identical in WT and KO mice, whereas *Rorgc* was slightly but significantly higher in the KO spleen at week 16 (Figure 6b). *Il-2* mRNA expression was significantly reduced only in the WT mice ($P < 0.002$). Because the expression of TSLP is mainly epithelial derived, *Tslp* mRNA expression was not observed in the spleen (data not shown). *Il-13rα1* was slightly elevated in WT mice, and *Il-13rα2* was significantly decreased in both mouse lines (untreated vs. 16-week treatment: $P < 0.009$ for WT and $P < 0.015$ for KO, Supplementary Figure S11b), indicating that lack of *Il-13rα1* does not result in compensatory upregulation of *Il-13rα2* expression.

## DISCUSSION

We have studied the effect of *Il-13rα1* deficiency on chemically induced skin papillomas and show that *Il-13rα1* protects against tumor development. As described previously in *Il-4*–, *Il-13*–, and *Il-4rα*–deficient mice (Rothe et al., 2013), IL-13–mediated signaling plays a critical defensive role against papilloma formation in response to chemical exposure in the skin. Interestingly, *Il-13rα1* mRNA expression was suppressed in the papillomas of WT mice, indicating that the chemically induced carcinogenesis possibly targets protective *Il-13rα1*, resulting in its downregulation.

Skin responds to environmental stress such as exposure to an allergen or a carcinogen by induction of danger signals, IL-25, IL-33, and TSLP (Hong et al., 2020; Roan et al., 2019). Of these, the expression of TSLP dramatically peaked at 2 weeks both in the serum and skin. TSLP level was significantly higher in KO mice. The role of TSLP in cancer is complex. Although TSLP promotes tumor progression by inducing predominant T helper 2–type inflammation (Protti and De Monte, 2020), it may provide an antitumor environment in the early stages of cancer development (Demehri et al., 2012). However, several reports highlight the protective role of TSLP against skin cancer; in the skin, for example, TSLP directly regulates CD4 and CD8 cells that in turn inhibit the recruitment of CD11b+Gr1+ myeloid cells that induce tumor growth (Di Piazza et al., 2012). TSLP provided protection against DMBA/TPA-induced papillomas in experimental atopic dermatitis model (Cipolat et al., 2014), and TSLP induction participates in the activation of CD4 T cells and possibly protection against skin cancer in actinic keratosis (Cunningham et al., 2017).

The possible mechanism of action on how the elevated TSLP in KO mice could influence tumor development might involve Tregs. Namely, TSLP can indirectly expand Tregs likely through dendritic cell activation (Leichner et al., 2017). In theory, the elevated TSLP in KO mice could explain the elevated number of Tregs. IL-2 is critical for both Treg differentiation and suppressive function (Chinen et al., 2016). In line with this, *Il-13rα1*–deficient mice had higher IL-2 expression and more Tregs than WT mice during papilloma formation. Thus, sustained IL-2 expression and elevated TSLP expression could be factors that explain the higher number of Tregs observed in KO mice. Tregs, in turn, express IL-10, which was downregulated in the WT but not in the KO mice. Interestingly, IL-10 expression suppresses tumor progression in experimental skin carcinogenesis (Mumm et al., 2011), but its high expression is an indicator of poor prognosis in patients with cancer (Zhao et al., 2015). Tregs regulate cancer cell growth in myriad ways, including local IL-2 consumption to downregulate CD4/CD8 and NK cells, downregulation of dendritic cell activation by the suppression of CD80/CD86, granzyme-mediated–targeted cell death, and metabolic inhibition of effector T-cell proliferation (Plitas and Rudensky, 2020). Recently, it was shown that CCR7-expressing dendritic cells that express CXCR6 ligand CXCL16 and *trans*-present IL-15 are critical for the survival and local expansion of CD8 cells to maximize their antitumor activity (Di Pilato et al., 2021). We found induction of both *Cxcr6* and *Ccr7* in the skin after 2-week DMBA/TPA treatment but found no difference in the expression between WT and KO mice, indicating that this pathway was not directly affected by IL-13Rα1.

Among the cytokines that can regulate and execute inflammation, IL-17 plays an important role in DMBA/TPA model (He et al., 2012; Wang et al., 2010). Closely linked IL-22 acts on epithelial and nonhematopoietic cells (Zenewicz, 2018) and supports epithelial regeneration and inflammation

(Ihekweazu et al., 2021; Mihi et al., 2021). Lack of IL-13Rα1—mediated signaling decreased IL-22 expression in the skin during papilloma induction. The role IL-22 plays in epithelial homeostasis is complex as shown in recent work decoupling the regenerative and proinflammatory functions of the cytokine by genetic recombineering (Saxton et al., 2021). In an experimental UV-induced squamous cell carcinoma model, anti–IL-22 reduces tumor number and burden (Abikhair et al., 2016), whereas direct IL-22 administration exacerbates aggressivity of squamous cell carcinoma cells (Abikhair Burgo et al., 2018). Our finding of decreased IL-22 in the *Il-13rα1*–KO mouse with increased papillomas underlines the complex role of IL-22 in cancer. This may have to do with the stage of tumor development that IL-22 regulates (Lim and Savan, 2014) or further delineated by the transcription factor, *Ror*γt (Lewis et al., 2021).

Aberrant cancer growth requires oxygen and nutrients, which are supplied by neovasculature (D'Amico et al., 2020; Mukwaya et al., 2021). Angiogenesis was compromised in the KO mice because the lumen of the blood vessels did not dilate as in WT mice, suggesting compromised intussusceptive angiogenesis (D'Amico et al., 2020). Both mouse strains seem to have a similar response to hypoxia, evidenced by similar expression of VEGF-A, and accordingly, sprouting angiogenesis is not defective in the KO strain. IL-13 is needed for transcription factor (GATA4)-induced angiogenesis in hypoxia (Malek Mohammadi et al., 2017), implying that *Il-13rα1* might regulate intussusceptive angiogenesis. The retarded angiogenesis in KO mice could also influence the immune response in the tumor model. Namely, if the KO mice did not have the same delivery of oxygen as WT mice, the tumor would become hypoxic and might facilitate the recruitment of immunosuppressive cells into the tumor (DePeaux and Delgoffe, 2021; Lee et al., 2020). This is essentially the skewed immunophenotype in KO mice.

Our results show the protective role of IL-13Rα1–mediated signaling against DMBA/TPA-induced skin papilloma formation. The protective role of IL-13Rα1 was linked to immunosuppressive cells. This highlights the complex role IL-13 plays in regulating inflammation and immune tolerance in the skin and warrant further studies on type II IL-4 receptor signaling, angiogenesis, and peripheral tolerance.

## MATERIALS AND METHODS

### Mice

*Il-13rα1*–KO mice on Balb/c background from Regeneron Pharmaceuticals (Tarrytown, NY) with age- and sex-matched WT Balb/c mice were used (Ramalingam et al., 2008). The WT mice were nonlittermates, were housed in the same animal room (identical light–dark cycle, feed, water, and handling), and were born within 4 days of the KOs. Mice were fed with standard laboratory pellets and water ad libitum. All animal experiments were performed under animal permit (ESAVI/23659/2018) by the National Animal Ethics Committee of Finland.

### Skin tumor induction

Both KO and control WT mice were treated with DMBA and TPA to induce skin tumors (Vähätupa et al., 2019). Briefly, the backs mice aged 8 weeks were shaved, and 24 or 48 hours later, 50 μg DMBA (Sigma-Aldrich, Dorset, United Kingdom) in 200 μl acetone was applied topically on the shaved area. A week later, the back skin was treated twice a week with 5 μg TPA (Sigma-Aldrich) in 100–200 μl acetone for 1 or 15 weeks. Fur (excluding tumors) was shaved every 2 weeks. Tumors (1 mm in diameter or larger) were counted weekly and marked on a separate tumor map, and changes in tumor development were individually recorded. The mice were anesthetized for handling with 4% isoflurane (Attane vet 1,000 mg/g, Piramal Critical Care B.V., Voorschoten, The Netherlands) carried by a mixture of 100% oxygen (0.2 l/min) and room air (0.4 l/min). The anesthesia was maintained with 2% isoflurane with the same gas mixture. From week 7, the mice were awakened during the second TPA pipetting but anesthetized for papilloma counting. The last TPA was pipetted 6–10 hours (in 16-week treatment) or 48 hours (in 2-week treatment) before being killed by carbon dioxide. Subsequently, tissue samples were collected. Negative controls of the antibodies used for immunohistochemistry staining are shown in Supplementary Figure S12.

### Statistical analysis

All data were analyzed to determine whether they were normally distributed, and then the significance was calculated by two-tailed Student's *t*-test for normally distributed data in most of the cases and with Mann–Whitney U test for values not normally distributed. In the histology analysis, logarithmic or square root transformation was used to normalize the distribution when needed. A significance level $<0.05$ was considered significant. Tumor-free survival plot data were analyzed by log-rank test (Mantel–Cox) model, and the non-normally distributed time course papilloma data were analyzed by nonlinear regression. IBM SPSS (version 25/26) was used for most analyses, and Prism 8/9 (GraphPad Software, La Jolla, CA) was used for the rest and in creating the charts.

### Supplementary methods

Standard methods (immunohistochemistry, quantitative analysis of immunohistochemical and histochemical stainings, flow cytometry, extraction of RNA and qPCR analysis, and ELISA and LUMINEX assays) are described in Supplementary Materials and Methods.

### Data availability statement

No datasets were generated or analyzed during this study.

### ORCIDs

Tanja Salomaa: http://orcid.org/0000-0003-4213-3066
Toini Pemmari: http://orcid.org/0000-0002-5822-8556
Juuso Määttä: http://orcid.org/0000-0001-6908-3383
Laura Kummola: http://orcid.org/0000-0003-3285-3668
Niklas Salonen: http://orcid.org/0000-0002-2809-063X
Martín González-Rodríguez: http://orcid.org/0000-0001-9434-0636
Liisa Parviainen: http://orcid.org/0000-0002-0263-2453
Lotta Hiihtola: http://orcid.org/0000-0002-4144-3559
Maria Vähätupa: http://orcid.org/0000-0002-7214-4527
Tero A.H. Järvinen: http://orcid.org/0000-0002-4027-1759
Ilkka S. Junttila: http://orcid.org/0000-0002-9830-0823

### AUTHOR CONTRIBUTIONS

Conceptualization: TAHJ, ISJ; Formal Analysis: TS, TP, JM, LK, NS, LP, MGR, LH, MV; Funding Acquisition: TAHJ, ISJ; Investigation: TS, TP, JM, LK, NS, LP, MGR, LH, MV; Supervision: TAHJ, ISJ; Writing - Original Draft Preparation: TS, TP, TAHJ, ISJ; Writing -Review and Editing: TS, TP, TAHJ, ISJ

### CONFLICT OF INTEREST

The authors state no conflict of interest.

### ACKNOWLEDGMENTS

This work was supported by the Academy of Finland (grants 25013080481 to ISJ, 25013142041, 287907 to TJ), The Competitive State Research Financing of the Expert Responsibility Area of Fimlab Laboratories (grant X51409 to ISJ), Tampere University Hospital (grants 9X011 and 9V010 to TJ), Päivikki and

Sakari Sohlberg Foundation (to TJ), Tampere University Hospital Support Foundation (to ISJ and TJ), Tampere Tuberculosis Foundation (to ISJ and TJ), Emil Aaltonen Foundation (to TP), and Paulo Foundation (to TP). The authors want to thank Marianne Karlsberg and Marja-Leena Koskinen for their excellent technical help. Regeneron Pharmaceuticals is thanked for providing the *Il13rα1*$^{-/-}$ mice.Additional correspondence may be addressed to Tero A.H. Järvinen, Faculty of Medicine and Health Technology, Tampere University, Arvo Ylpönkatu 34, 33250 Tampere, Finland. Email: tero.jarvinen@tuni.fi.

## SUPPLEMENTARY MATERIAL

Supplementary material is linked to the online version of the paper at www.jidonline.org, and at https://doi.org/10.1016/j.jid.2021.11.013.

## REFERENCES

Abel EL, Angel JM, Kiguchi K, DiGiovanni J. Multi-stage chemical carcinogenesis in mouse skin: fundamentals and applications. Nat Protoc 2009;4:1350–62.

Abikhair Burgo M, Roudiani N, Chen J, Santana AL, Doudican N, Proby C, et al. Ruxolitinib inhibits cyclosporine-induced proliferation of cutaneous squamous cell carcinoma. JCI Insight 2018;3:e120750.

Abikhair M, Mitsui H, Yanofsky V, Roudiani N, Ovits C, Bryan T, et al. Cyclosporine A immunosuppression drives catastrophic squamous cell carcinoma through IL-22. JCI Insight 2016;1:e86434.

Akkaya B, Shevach EM. Regulatory T cells: master thieves of the immune system. Cell Immunol 2020;355:104160.

Andrews AL, Holloway JW, Puddicombe SM, Holgate ST, Davies DE. Kinetic analysis of the interleukin-13 receptor complex. J Biol Chem 2002;277:46073–8.

Barsheshet Y, Wildbaum G, Levy E, Vitenshtein A, Akinseye C, Griggs J, et al. CCR8+FOXp3+ Treg cells as master drivers of immune regulation. Proc Natl Acad Sci USA 2017;114:6086–91.

Bolontrade MF, Stern MC, Binder RL, Zenklusen JC, Gimenez-Conti IB, Conti CJ. Angiogenesis is an early event in the development of chemically induced skin tumors. Carcinogenesis 1998;19:2107–13.

Chinen T, Kannan AK, Levine AG, Fan X, Klein U, Zheng Y, et al. An essential role for the IL-2 receptor in Treg cell function. Nat Immunol 2016;17:1322–33.

Cipolat S, Hoste E, Natsuga K, Quist SR, Watt FM. Epidermal barrier defects link atopic dermatitis with altered skin cancer susceptibility. Elife 2014;3:e01888.

Cunningham TJ, Tabacchi M, Eliane JP, Tuchayi SM, Manivasagam S, Mirzaalian H, et al. Randomized trial of calcipotriol combined with 5-fluorouracil for skin cancer precursor immunotherapy. J Clin Invest 2017;127:106–16.

Dalessandri T, Crawford G, Hayes M, Castro Seoane R, Strid J. IL-13 from intraepithelial lymphocytes regulates tissue homeostasis and protects against carcinogenesis in the skin. Nat Commun 2016;7:12080.

D'Amico G, Muñoz-Félix JM, Pedrosa AR, Hodivala-Dilke KM. "Splitting the matrix": intussusceptive angiogenesis meets MT1-MMP. EMBO Mol Med 2020;12:e11663.

De Rossi G, Vähätupa M, Cristante E, Arokiasamy S, Liyanage SE, May U, et al. Pathological angiogenesis requires syndecan-4 for efficient VEGFA-induced VE-cadherin internalization. Arterioscler Thromb Vasc Biol 2021;41:1374–89.

Demehri S, Turkoz A, Manivasagam S, Yockey LJ, Turkoz M, Kopan R. Elevated epidermal thymic stromal lymphopoietin levels establish an antitumor environment in the skin. Cancer Cell 2012;22:494–505.

DePeaux K, Delgoffe GM. Metabolic barriers to cancer immunotherapy [e-pub ahead of print]. Nat Rev Immunol 2021; https://doi.org/10.1038/s41577-021-00541-y (accessed October 10, 2021).

Di Piazza M, Nowell CS, Koch U, Durham AD, Radtke F. Loss of cutaneous TSLP-dependent immune responses skews the balance of inflammation from tumor protective to tumor promoting. Cancer Cell 2012;22:479–93.

Di Pilato M, Kfuri-Rubens R, Pruessmann JN, Ozga AJ, Messemaker M, Cadilha BL, et al. CXCR6 positions cytotoxic T cells to receive critical survival signals in the tumor microenvironment. Cell 2021;184. 4512–30.e22.

Dunn GP, Old LJ, Schreiber RD. The immunobiology of cancer immunosurveillance and immunoediting. Immunity 2004;21:137–48.

Fichtner-Feigl S, Strober W, Kawakami K, Puri RK, Kitani A. IL-13 signaling through the IL-13alpha2 receptor is involved in induction of TGF-beta1 production and fibrosis. Nat Med 2006;12:99–106.

Gabrilovich DI, Nagaraj S. Myeloid-derived suppressor cells as regulators of the immune system. Nat Rev Immunol 2009;9:162–74.

Gonzalez H, Hagerling C, Werb Z. Roles of the immune system in cancer: from tumor initiation to metastatic progression. Genes Dev 2018;32:1267–84.

He D, Li H, Yusuf N, Elmets CA, Athar M, Katiyar SK, et al. IL-17 mediated inflammation promotes tumor growth and progression in the skin. PLoS One 2012;7:e32126.

Henderson NC, Rieder F, Wynn TA. Fibrosis: from mechanisms to medicines. Nature 2020;587:555–66.

Hiam-Galvez KJ, Allen BM, Spitzer MH. Systemic immunity in cancer. Nat Rev Cancer 2021;21:345–59.

Hong H, Liao S, Chen F, Yang Q, Wang DY. Role of IL-25, IL-33, and TSLP in triggering united airway diseases toward type 2 inflammation. Allergy 2020;75:2794–804.

Ihekweazu FD, Engevik MA, Ruan W, Shi Z, Fultz R, Engevik KA, et al. Bacteroides ovatus promotes IL-22 production and reduces trinitrobenzene sulfonic acid–driven colonic inflammation. Am J Pathol 2021;191:704–19.

Jeannin P, Paolini L, Adam C, Delneste Y. The roles of CSFs on the functional polarization of tumor-associated macrophages. FEBS J 2018;285:680–99.

Junttila IS, Mizukami K, Dickensheets H, Meier-Schellersheim M, Yamane H, Donnelly RP, et al. Tuning sensitivity to IL-4 and IL-13: differential expression of IL-4Ralpha, IL-13Ralpha1, and gammac regulates relative cytokine sensitivity. J Exp Med 2008;205:2595–608.

Kaviratne M, Hesse M, Leusink M, Cheever AW, Davies SJ, McKerrow JH, et al. IL-13 activates a mechanism of tissue fibrosis that is completely TGF-beta independent. J Immunol 2004;173:4020–9.

LaPorte SL, Juo ZS, Vaclavikova J, Colf LA, Qi X, Heller NM, et al. Molecular and structural basis of cytokine receptor pleiotropy in the interleukin-4/13 system. Cell 2008;132:259–72.

Lee CG, Homer RJ, Zhu Z, Lanone S, Wang X, Koteliansky V, et al. Interleukin-13 induces tissue fibrosis by selectively stimulating and activating transforming growth factor beta(1). J Exp Med 2001;194:809–21.

Lee WS, Yang H, Chon HJ, Kim C. Combination of anti-angiogenic therapy and immune checkpoint blockade normalizes vascular-immune crosstalk to potentiate cancer immunity. Exp Mol Med 2020;52:1475–85.

Leichner TM, Satake A, Harrison VS, Tanaka Y, Archambault AS, Kim BS, et al. Skin-derived TSLP systemically expands regulatory T cells. J Autoimmun 2017;79:39–52.

Lewis JM, Monico PF, Mirza FN, Xu S, Yumeen S, Turban JL, et al. Chronic UV radiation-induced RORγt+ IL-22-producing lymphoid cells are associated with mutant KC clonal expansion. Proc Natl Acad Sci USA 2021;118:e2016963118.

Li C, Jiang P, Wei S, Xu X, Wang J. Regulatory T cells in tumor microenvironment: new mechanisms, potential therapeutic strategies and future prospects. Mol Cancer 2020;19:1–116.

Li S, Park H, Trempus CS, Gordon D, Liu Y, Cotsarelis G, et al. A keratin 15 containing stem cell population from the hair follicle contributes to squamous papilloma development in the mouse. Mol Carcinog 2013;52:751–9.

Lim C, Savan R. The role of the IL-22/IL-22R1 axis in cancer. Cytokine Growth Factor Rev 2014;25:257–71.

Malek Mohammadi M, Kattih B, Grund A, Froese N, Korf-Klingebiel M, Gigina A, et al. The transcription factor GATA4 promotes myocardial regeneration in neonatal mice [published correction appears in EMBO Mol Med 2019;11:e10678]. EMBO Mol Med 2017;9:265–79.

Mihi B, Gong Q, Nolan LS, Gale SE, Goree M, Hu E, et al. Interleukin-22 signaling attenuates necrotizing enterocolitis by promoting epithelial cell regeneration. Cell Rep Med 2021;2:100320.

Mittal D, Gubin MM, Schreiber RD, Smyth MJ. New insights into cancer immunoediting and its three component phases–elimination, equilibrium and escape. Curr Opin Immunol 2014;27:16–25.

Mukwaya A, Jensen L, Lagali N. Relapse of pathological angiogenesis: functional role of the basement membrane and potential treatment strategies. Exp Mol Med 2021;53:189–201.

Mumm JB, Emmerich J, Zhang X, Chan I, Wu L, Mauze S, et al. IL-10 elicits IFNγ-dependent tumor immune surveillance. Cancer Cell 2011;20:781–96.

Plitas G, Rudensky AY. Regulatory T cells in cancer. Annu Rev Cancer Biol 2020;4:459–77.

Protti MP, De Monte L. Thymic stromal lymphopoietin and cancer: Th2-dependent and -independent mechanisms. Front Immunol 2020;11:2088.

Ramalingam TR, Pesce JT, Sheikh F, Cheever AW, Mentink-Kane MM, Wilson MS, et al. Unique functions of the type II interleukin 4 receptor identified in mice lacking the interleukin 13 receptor alpha1 chain. Nat Immunol 2008;9:25–33.

Roan F, Obata-Ninomiya K, Ziegler SF. Epithelial cell-derived cytokines: more than just signaling the alarm. J Clin Invest 2019;129:1441–51.

Rothe M, Quarcoo D, Chashchina AA, Bozrova SV, Qin Z, Nedospasov SA, et al. IL-13 but not IL-4 signaling via IL-4Rα protects mice from papilloma formation during DMBA/TPA two-step skin carcinogenesis. Cancer Med 2013;2:815–25.

Saxton RA, Henneberg LT, Calafiore M, Su L, Jude KM, Hanash AM, et al. The tissue protective functions of interleukin-22 can be decoupled from pro-inflammatory actions through structure-based design. Immunity 2021;54:660–72.e9.

Vähätupa M, Pemmari T, Junttila I, Pesu M, Järvinen TAH. Chemical-induced skin carcinogenesis model using dimethylbenz[a]anthracene and 12-O-tetradecanoyl phorbol-13-acetate (DMBA-TPA). J Vis Exp 2019;154.

Veglia F, Perego M, Gabrilovich D. Myeloid-derived suppressor cells coming of age. Nat Immunol 2018;19:108–19.

Wang L, Yi T, Zhang W, Pardoll DM, Yu H. IL-17 enhances tumor development in carcinogen-induced skin cancer. Cancer Res 2010;70:10112–20.

Wills-Karp M, Luyimbazi J, Xu X, Schofield B, Neben TY, Karp CL, et al. Interleukin-13: central mediator of allergic asthma. Science 1998;282:2258–61.

Zenewicz LA. IL-22: there is a gap in our knowledge. Immunohorizons 2018;2:198–207.

Zhao S, Wu D, Wu P, Wang Z, Huang J. Serum IL-10 predicts worse outcome in cancer patients: a meta-analysis. PLoS One 2015;10:e0139598.

## SupplementaryMaterials AND METHODS

### Immunohistochemistry

Samples of back skin from killed, shaved, and untreated mice or mice at week 2 or 16 after 7,12-dimethylbenz[*a*]anthracene/12-*O*-tetradecanoyl phorbol-13-acetate treatment were collected and fixed with 4% paraformaldehyde in PBS and embedded in paraffin according to standard protocols. Hematoxylin staining and 3,3′-diaminobenzidine immunohistochemical staining were performed on paraffin sections as previously described (May et al., 2015; Vähätupa et al., 2016). The following primary antibodies were used for immunohistochemistry (according to the manufacturer's instructions): IHC-00375 rabbit anti-mouse Ki-67 (Bethyl Laboratories, Montgomery, TX), ab68672 rabbit anti-mouse neutrophil elastase (Abcam, Oxford, United Kingdom), MF48000 rat anti-mouse F4/80 (Invitrogen, Waltham, MA), A0452 rabbit anti-human CD3 (Dako, Glostrup, Denmark), 550274 rat anti-mouse CD31 (BD Pharmingen, Franklin Lakes, NJ), ab181548 rabbit anti-mouse integrin alpha 2 (CD49b, Abcam), HS-361 003 rabbit anti-mouse CD8a (Synaptic Systems, Goettingen, Germany), and NB100-39002 rabbit anti-mouse Foxp3 (Novus Biologicals, Abingdon, United Kingdom). The blocking reagent used was S2023 Real Peroxidase Blocking Solution (Dako). The horseradish peroxidase–conjugated secondary antibodies were P0448 goat anti-rabbit (Dako) (for Ki-67, CD3, and Foxp3) and RMR622H Rabbit on Rodent Horseradish Peroxidase Polymer (Biocare Medical, Concord, CA) (for neutrophil elastase and CD8). The 414311F Histofine Simple stain Mouse Max PO (rat) (Nichirei Biosciences, Tokyo, Japan) was used as a secondary antibody for F4/80 and CD31 stainings, and 414341F Histofine Simple stain Mouse Max PO (R) (Nichirei Biosciences) was used for integrin alpha 2 stainings. The peroxidase reactive chromogen K3468 3,3′-diaminobenzidine + substrate Chromogen System (Dako) was used as instructed by the manufacturer. The specificity of the secondary antibodies was ensured with stainings lacking the primary antibody (Supplementary Figure S12).

### Quantitative analysis of immunostaining and histochemical staining

All slides were scanned using the NanoZoomer S60 (Hamamatsu Photonics, Hamamatsu City, Japan). Slides were viewed and analyzed in a blinded fashion using QuPath software, version 0.2.0 or later (Bankhead et al., 2017). The area of interest was chosen with QuPath brush tool. The samples were analyzed in their entirety, excluding technically compromised areas, and the magnification was adjusted constantly to ensure as an accurate choice of area of interest as possible. Positive cell detection function was applied to quantify the immunohistochemical signal, and the algorithm settings were kept the same during the analysis of one antibody. The percentage of positive cells of all cells in the measured area was recorded except for the CD31 density analysis, where the number of positive cells in ratio to the whole area measured was recorded, and the CD3, CD8, and Foxp3 hair bulge analysis, where a hair bulge was considered as positive if it contained one or more 3,3′-diaminobenzidine–stained cells and was considered negative otherwise. On average, 5,200 cells from dermal areas, 2,700 cells from epidermal areas, and 8,400 cells from papillomas were counted from one sample. The average areas analyzed were 1.19 $mm^2$ (dermis), 0.26 $mm^2$ (dermis), and 1.82 $mm^2$ (papillomas) per sample. The average amount of analyzes for appendage structures per sample was 24 for hair bulges and 27 for sebaceous glands. The lumen diameters and epidermal and dermal thicknesses were measured with QuPath Line tool. On average, 200 vessels were measured and averaged from every sample. The epidermal and dermal thicknesses were measured nine times per sample and averaged. The measurements were taken from areas where no papilloma formation was detected, and the sample was cut as perpendicular to the skin surface as possible. The perpendicularity was assessed on the basis of the appearance of the skin appendages, that is, hair follicles and associated structures. The sample lengths for the neutrophil cluster analysis were measured with NDP.view2 software (version 2.8.24, Hamamatsu Photonics).

### Extraction of RNA and qPCR analysis

Samples of back skin were harvested into RNAlater RNA Stabilization Reagent (Qiagen, Hilden, Germany) and snap frozen in liquid nitrogen. The mRNA was extracted using Invitrogen Trizol Reagent (Thermo Fisher Scientific, Waltham, MA) according to the manufacturer's instructions. Homogenization was performed with Precellys homogenizer (Precellys, Yvelines, France) in CKMix tubes. The skin samples were homogenized at 6,500 r.p.m. for 2 minutes in total and the other samples for a minute. The RNA extraction from the skin samples was done with E.Z.N.A. Total RNA Kit I (VWR, Radnor, PA) and from the spleen samples with RNeasy Fibrous Tissue Mini Kit (Qiagen) according to the manufacturer's instructions. The amount of RNA was measured using NanoDrop One (Thermo Fisher Scientific), and its quality was checked with gel electrophoresis. RNA was converted to cDNA by reverse transcription using the Thermo Maxima First Strand cDNA Synthesis Kit for RT-qPCR (Thermo Fisher Scientific) according to the manufacturer's instructions. A total of 50 ng of cDNA was used for qPCR analysis, which was performed in MicroAmp Fast Optical 96-well reaction plate (Applied Biosystems, Foster City, CA) in a QuantStudio 12K Flex Real-Time PCR System (Applied Biosystems). The qPCR reaction was done in a reaction volume of 20 μl with Luna Universal qPCR Master Mix (New England BioLabs, Ipswich, MA) according to the manufacturer's instructions with primers for *Foxp3, Tbet, Rorγc, Arg1, Gata3, Il-4, Il-13, Il-10, Il-15, Tgfβ, Il-4rα, Il-7r, Tslpr, Cxcl16, Cxcr6, Ccr7, Camp, Defb4, Lcn2*, and *Ifnγ* (all 250 nM) and for the reference gene *18S* (250 nM). Supplementary Table S3 provides the primer sequences used. Antarctic Thermolabile UDG (0.0125 units/μl) (ArticZymes, Tromsø, Norway) was used in reactions to prevent possible contamination between the runs. For *Tslp, Il-2, Ccl1, Ccr8, Il-13rα1*, And *Il-13rα2* determination, TaqMan Fast Advanced MasterMix was used with specific probes (Mm01157588_m1 for *Tslp*, Mm00434256_m for *Il-2*, Mm99999220_mH for *Ccl1*, Mm01351703_m1 for *Ccr8*, Mm00446726_m1 for *Il-13rα1*, and Mm00515166_m1 for *Il-13rα2*, all from Applied Biosystems) in 20 μl reaction volume. As negative controls, no-template and no-reverse transcriptase controls were also

included. The thermal cycler profile for all primer-based sets was 10 minutes 25 °C, 1 minute 95 °C, ×40 (15 seconds 95 °C, 30 seconds 60 °C + plate read). At the end of the thermal program, a melting curve analysis was always performed to check unspecific PCR. For TaqMan assays, the thermal cycler profile set was for 2 minutes at 50 °C, 2 minutes at 95 °C, ×40 (1 second 95 °C, 20 seconds at 60 °C). DeltadeltaCt method was used to analyze the data. In addition, for better visualization, the relative gene expression is shown relative to the condition wild-type untreated.

**ELISA and LUMINEX assays**

Cytokine and chemokine determination was performed from serum and skin or papilloma samples. The untreated mice and mice treated with 7,12-dimethylbenz[*a*]anthracene/12-*O*-tetradecanoyl phorbol-13-acetate for 2 or 16 weeks were killed, and sera were collected and stored at −20 °C before the assay. Skin and papilloma samples from the back were collected right after killing and then immediately frozen with liquid nitrogen. Before the assay, skin and papilloma samples were lysed in 200 μl of cold RIPA Lysis and Extraction Buffer (Thermo Fisher Scientific) with added 10 μl/ml Halt Phosphatase Inhibitor Cocktail (Thermo Fisher Scientific). Homogenization was performed with Precellys homogenizer (Precellys) in CKMix50 tubes. The skin and papilloma samples were homogenized at 6,500 r.p.m. for a total of 1 minute. Lysates were then centrifuged at 16,000*g* for 10 minutes at 4 °C, and the supernatant was collected. The protein concentration of the supernatants was determined by Pierce Protein BCA assay kit (Thermo Fisher Scientific). To determine cytokine/chemokine levels in the skin or papilloma samples and serums, Invitrogen ProCartaPlex assay (custom-made 22-plex panel, Thermo Fisher Scientific) was used according to the manufacturer's instructions with Bio-Plex 200 instrument (Bio-Rad Laboratories, Hercules, CA). Measured cytokines and chemokines in the panel were IL-1α, IL-1β, IL-2, IL-4, IL-5, IL-6, IL-7, IL-10, IL-13, IL-17A, IL-18, IL-21, IL-22, IL-25, IL-27, IL-33, TSLP, IFNγ, TNF, CXCL10, VEGF-A, and CCL5. Detected protein amounts were normalized with the total protein concentration (determined by BCA). To detect TGF-β1 from serum samples, Invitrogen TGFβ1 Human/Mouse Uncoated ELISA Kit (Thermo Fisher Scientific) was used according to the manufacturer's instructions.

**Flow cytometry**

The untreated mice and mice treated with 7,12-dimethylbenz[*a*]anthracene/12-*O*-tetradecanoyl phorbol-13-acetate for 2 or 16 weeks were killed, and the spleens and draining lymph nodes were collected. Organs were mashed on a Petri dish in PBS containing 2 mM EDTA (Sigma-Aldrich, Dorset, United Kingdom) and 0.1% BSA (Sigma-Aldrich), filtered through a 40-μm strainer, and then centrifuged for 5 minutes at 350*g* at 4 °C to harvest single cells. For splenic cells, red blood cell lysis was performed with ACK lysing buffer (Gibco, Thermo Fisher Scientific). Samples were suspended into PBS and incubated with a viability dye (FVS510, BD Pharmingen) for 45 minutes at 4 °C. Then, samples were washed with PBS containing 2 mM EDTA and 0,1% BSA and incubated with mouse BD Fc Block (clone 2.4G2, BD Pharmingen) for 5 minutes at 4 °C. To analyze myeloid-derived suppressor cells, the skin draining lymph node cells and splenic cells were stained with antibodies against mouse CD11b (FITC, clone M1/70, BD Pharmingen), F4/80 (phycoerythrin-Cy7, clone BM8, Thermo Fisher Scientific), CD11c (PerCP-5.5, clone HL3, BD Pharmingen), major histocompatibility complex II (allophycocyanin, clone M5/114.15.2, Thermo Fisher Scientific), Ly6G (allophycocyanin-Cy7, clone 1A8, BD Pharmingen), Ly6C (phycoerythrin-CF594, clone AL-21, BD Pharmingen), CD115 (BV421, clone AFS98, BioLegend, San Diego, CA), and CD124 (phycoerythrin, clone mIL4R-M1, BD Pharmingen). Cells were incubated for 20 minutes at 4 °C and washed twice with PBS containing 2 mM EDTA and 0.1% BSA before flow cytometric analysis. For intracellular Foxp3 staining, isolated draining lymph node and splenic cells were first stained with FVS510 in PBS for 45 minutes at 4 °C and washed with PBS containing 2 mM EDTA and 0.1% BSA, followed by incubation with mouse BD Fc Block for 5 minutes at 4 °C. Surface staining was then performed for 20 minutes at 4 °C with the following antibodies: CD3 (FITC, clone 17A2, BD Pharmingen), CD8 (allophycocyanin-H7, clone 53-6.7, BD Pharmingen), CD127 (phycoerythrin-Cy7, clone SB/199, BD Pharmingen), and CD25 (AlexaFluor 647, clone 7D4, BD Pharmingen). Cells were then fixed and permeabilized using the Mouse Foxp3 Buffer Set (BD Pharmingen) according to manufacturer instructions and stained with antibodies for Foxp3 (phycoerythrin, clone MF23, BD Pharmingen) and CD4 (PerCP-Cy5.5, clone RM4-5, BD Pharmingen) for 20 minutes at room temperature. Cells were washed twice with PBS containing 2 mM EDTA and 0.1% BSA before flow cytometric analysis. All cells were analyzed with FACSAria Fusion (BD Pharmingen), and data analysis was performed with FlowJo software (Flowjo, Ashland, Oregon).

## SUPPLEMENTARY REFERENCES

Bankhead P, Loughrey MB, Fernández JA, Dombrowski Y, McArt DG, Dunne PD, et al. QuPath: open source software for digital pathology image analysis. Sci Rep 2017;7:16878.

May U, Prince S, Vähätupa M, Laitinen AM, Nieminen K, Uusitalo-Järvinen H, et al. Resistance of R-ras knockout mice to skin tumour induction. Sci Rep 2015;5:11663.

Vähätupa M, Aittomäki S, Martinez Cordova Z, May U, Prince S, Uusitalo-Järvinen H, et al. T-cell-expressed proprotein convertase FURIN inhibits DMBA/TPA-induced skin cancer development. Oncoimmunology 2016;5:e1245266.

## Supplementary Table S1. Statistically Significant P-Values of Indicated Treatment Groups in Mouse Strains, Calculated by Mann–Whitney U Test

| | | Serum | | | Skin | | |
|---|---|---|---|---|---|---|---|
| **Cytokine** | **Mouse Line** | **0 wk Versus 16 wk** | **0 wk Versus 2 wk** | **2 wk Versus 16 wk** | **0 wk Versus 16 wk** | **0 wk Versus 2 wk** | **2 wk Versus 16 wk** |
| IL-1β | WT | n.s. | n.s. | n.s. | 0.05 | n.s. | n.s. |
| | KO | n.s. | n.s. | n.s. | 0.001 | 0.000 | 0.01 |
| IL-2 | WT | n.s. | n.s. | n.s. | 0.018 | 0.011 | n.s. |
| | KO | n.s. | n.s. | n.s. | 0.000 | 0.036 | 0.013 |
| IL-4 | WT | n.s. | n.s. | n.s. | 0.001 | 0.005 | 0.008 |
| | KO | n.s. | n.s. | n.s. | 0.000 | 0.000 | 0.000 |
| IL-5 | WT | n.s. | n.s. | n.s. | n.s. | n.s. | 0.008 |
| | KO | 0.02 | n.s. | n.s. | n.s. | 0.001 | 0.000 |
| IL-6 | WT | n.s. | n.s. | 0.001 | 0.05 | 0.000 | n.s. |
| | KO | n.s. | 0.000 | 0.006 | 0.007 | n.s. | n.s. |
| IL-7 | WT | n.s. | 0.003 | n.s. | 0.026 | 0.022 | n.s. |
| | KO | n.s. | n.s. | n.s. | 0.001 | n.s. | 0.006 |
| IL-10 | WT | n.s. | n.s. | 0.005 | 0.036 | 0.022 | n.s. |
| | KO | n.s. | n.s. | n.s. | 0.003 | 0.026 | n.s. |
| IL-13 | WT | n.s. | n.s. | n.s. | n.s. | n.s. | n.s. |
| | KO | 0.008 | n.s. | 0.043 | n.s. | n.s. | 0.043 |
| IL-17A | WT | 0.000 | n.s. | 0.000 | 0.000 | 0.005 | 0.001 |
| | KO | 0.003 | n.s. | 0.001 | 0.000 | 0.000 | 0.003 |
| IL-22 | WT | n.s. | n.s. | n.s. | 0.018 | 0.000 | 0.002 |
| | KO | n.s. | n.s. | n.s. | 0.000 | 0.000 | 0.008 |
| IL-25 | WT | n.s. | n.s. | n.s. | n.s. | n.s. | 0.028 |
| | KO | n.s. | n.s. | n.s. | n.s. | 0.002 | 0.000 |
| IL-33 | WT | n.s. | n.s. | n.s. | 0.012 | 0.003 | n.s. |
| | KO | n.s. | n.s. | n.s. | 0.000 | 0.001 | n.s. |
| IFNγ | WT | n.s. | 0.007 | 0.002 | n.s. | 0.031 | n.s. |
| | KO | n.s. | 0.002 | 0.001 | 0.005 | n.s. | 0.028 |
| TNF | WT | n.s. | n.s. | 0.011 | n.s. | n.s. | 0.003 |
| | KO | n.s. | n.s. | 0.012 | 0.031 | n.s. | n.s. |
| TSLP | WT | n.s. | 0.000 | 0.000 | 0.000 | 0.003 | 0.013 |
| | KO | 0.001 | 0.000 | 0.000 | 0.000 | 0.001 | 0.000 |
| TGFβ1 | WT | n.s. | n.s. | n.s. | n.m. | n.m. | n.m. |
| | KO | n.s. | 0.048 | n.s. | n.m. | n.m. | n.m. |
| VEGF-A | WT | n.s. | n.s. | n.s. | 0.000 | 0.031 | 0.000 |
| | KO | n.s. | n.s. | 0.021 | 0.000 | 0.001 | 0.000 |

Abbreviations: KO, knockout; n.m., not measured; n.s., not significant; wk, week; WT, wild-type.

## Supplementary Table S2. Statistically Significant P-Values of Indicated Treatment Groups in Mouse Strains, Calculated by Mann–Whitney U Test

| | | Skin | | | Spleen | | |
|---|---|---|---|---|---|---|---|
| **Gene** | **Mouse Line** | **0 wk Versus 16 wk** | **0 wk Versus 2 wk** | **2 wk Versus 16 wk** | **0 wk Versus 16 wk** | **0 wk Versus 2 wk** | **2 wk Versus 16 wk** |
| *Il-7r* | WT | n.m. | n.s. | n.m. | n.m. | n.m. | n.m. |
| | KO | n.m. | n.s. | n.m. | n.m. | n.m. | n.m. |
| *Tslpr* | WT | n.m. | n.s. | n.m. | n.m. | n.m. | n.m. |
| | KO | n.m. | n.s. | n.m. | n.m. | n.m. | n.m. |
| *Cxcl16* | WT | n.m. | 0.0238 | n.m. | n.m. | n.m. | n.m. |
| | KO | n.m. | n.s. | n.m. | n.m. | n.m. | n.m. |
| *Cxcr6* | WT | n.m. | 0.0238 | n.m. | n.m. | n.m. | n.m. |
| | KO | n.m. | n.s. | n.m. | n.m. | n.m. | n.m. |
| *Ccl1* | WT | 0.02381 | 0.0238 | 0.002165 | n.m. | n.m. | n.m. |
| | KO | 0.047619 | n.s. | 0.002165 | n.m. | n.m. | n.m. |
| *Ccr8* | WT | 0.002165 | 0.02381 | 0.0238 | n.m. | n.m. | n.m. |
| | KO | 0.004329 | 0.047619 | n.s. | n.m. | n.m. | n.m. |
| *Camp* | WT | n.s. | n.s. | n.s. | n.m. | n.m. | n.m. |
| | KO | n.s. | n.s. | n.s. | n.m. | n.m. | n.m. |
| *Defb4* | WT | 0.0238 | 0.0238 | 0.002165 | n.m. | n.m. | n.m. |
| | KO | 0.0238 | n.s. | 0.002165 | n.m. | n.m. | n.m. |
| *Lcn2* | WT | 0.0238 | 0.0238 | n.s. | n.m. | n.m. | n.m. |
| | KO | n.s. | n.s. | 0.002165 | n.m. | n.m. | n.m. |
| *Rorg* | WT | 0.0238 | 0.02381 | 0.041126 | 0.007 | n.m. | n.m. |
| | KO | n.s. | 0.047619 | n.s. | n.s. | n.m. | n.m. |
| *Tbet* | WT | 0.0238 | n.s. | 0.002165 | 0.007 | n.m. | n.m. |
| | KO | 0.0238 | n.s. | 0.002165 | 0.049 | n.m. | n.m. |
| *Gata3* | WT | 0.0238 | n.s. | 0.004329 | 0.029 | n.m. | n.m. |
| | KO | 0.0238 | 0.047619 | 0.002165 | n.s. | n.m. | n.m. |
| *Foxp3* | WT | n.s. | 0.0238 | 0.009524 | 0 | n.s. | 0.007 |
| | KO | n.s. | 0.0238 | 0.019048 | 0 | n.s. | 0.007 |
| *Ccr7* | WT | n.m. | 0.0238 | n.m. | n.m. | n.m. | n.m. |
| | KO | n.m. | 0.0238 | n.m. | n.m. | n.m. | n.m. |
| *Il-15* | WT | n.m. | n.s. | n.m. | n.m. | n.m. | n.m. |
| | KO | n.m. | n.s. | n.m. | n.m. | n.m. | n.m. |
| *Arg1* | WT | n.s. | n.m. | n.m. | n.s. | n.m. | n.m. |
| | KO | n.s. | n.m. | n.m. | n.s. | n.m. | n.m. |
| *Il-10* | WT | n.s. | n.m. | n.m. | n.s. | n.m. | n.m. |
| | KO | n.s. | n.m. | n.m. | n.s. | n.m. | n.m. |
| *Il-13* | WT | n.s. | n.m. | n.m. | n.s. | n.m. | n.m. |
| | KO | n.s. | n.m. | n.m. | n.s. | n.m. | n.m. |
| *Tslp* | WT | 0.047619 | 0.0238 | 0.041126 | n.d. | n.d. | n.d. |
| | KO | 0.02381 | 0.0238 | n.s. | n.d. | n.d. | n.d. |
| *Il-4rα* | WT | n.m. | n.m. | n.m. | n.s. | n.s. | n.s. |
| | KO | n.m. | n.m. | n.m. | n.s. | n.s. | n.s. |
| *Il-13rα1* | WT | n.s. | n.s. | 0.01 | 0.009 | n.s. | 0.009 |
| | KO | n.d. | n.d. | n.d. | n.d. | n.d. | n.d. |
| *Il-13rα2* | WT | n.s. | n.s. | 0.041 | 0.009 | n.s. | n.s. |
| | KO | n.s. | n.s. | 0.015 | 0.015 | n.s. | 0.015 |
| *Ifnγ* | WT | n.m. | n.m. | n.m. | 0.007 | n.m. | n.m. |
| | KO | n.m. | n.m. | n.m. | 0.007 | n.m. | n.m. |
| *Il-2* | WT | n.m. | n.m. | n.m. | 0.002 | 0.02 | 0.002 |
| | KO | n.m. | n.m. | n.m. | n.s. | 0.002 | 0.002 |
| *Tgfβ* | WT | n.m. | n.m. | n.m. | n.s. | 0.015 | 0.009 |
| | KO | n.m. | n.m. | n.m. | n.s. | n.s. | n.s. |
| *Il-4* | WT | n.m. | n.m. | n.m. | 0.049 | n.s. | n.s. |
| | KO | n.m. | n.m. | n.m. | n.s. | n.s. | n.s. |

Abbreviations: KO, knockout; n.d., not detected; n.m., not measured; n.s., not significant; wk, week; WT, wild-type.

## Supplementary Table S3. Sequences of qPCR Primers Used

| Gene Target | Primer Sequence | 5′–3′ |
|---|---|---|
| *Foxp3* | Forward | 5′-TCAGGAGCCCACCAGTACA-3′ |
| | Reverse | 5′-TCTGAAGGCAGAGTCAGGAGA-3′ |
| *Gata3* | Forward | 5′-TTATCAAGCCCAAGCGAAG-3′ |
| | Reverse | 5′-TGGTGGTGGTCTGACAGTTC-3′ |
| *Ifnγ* | Forward | 5′-GGAGGAACTGGCAAAAGGAT-3′ |
| | Reverse | 5′-TTCAAGACTTCAAAGAGT CTGAGG-3′ |
| *Il-2* | Forward | 5′-GCTGTTGATGGACCTACAGGA-3′ |
| | Reverse | 5′-TTCAATTCTGTGGCCTGCTT-3′ |
| *Il-4* | Forward | 5′-GAGAGATCATCGGCATTTTGA-3′ |
| | Reverse | 5′-AGCCCTACAGACGAGCTCAC-3′ |
| *Tbet (used for spleen samples)* | Forward | 5′- TCAACCAGCACCAGACAGAG-3′ |
| | Reverse | 5′-AAACATCCTGTAATGGCTTGTG-3′ |
| *Tbet (used for skin samples)* | Forward | 5′-GTTCCCATTCCTGTCCTTCAC-3′ |
| | Reverse | 5′-AGCTTCCCAAATGAAACTTCC-3′ |
| *Rorγc* | Forward | 5′-CACTGCCAGCTGTGTGCT-3′ |
| | Reverse | 5′-TGCAAGGGATCACTTCAATTT-3′ |
| *Il-17a* | Forward | 5′-CAGGGAGAGCTTCATCTGTGT-3′ |
| | Reverse | 5′-GCTGAGCTTTGAGGGATGAT-3′ |
| *Inos2* | Forward | 5′-GGGCAGTGGAGAGATTTTGC-3′ |
| | Reverse | 5′-CCAGAGGGGTAGGCTTGTCT-3′ |
| *Arg1* | Forward | 5′-AAGAATGGAAGAGTCAGTGTGG-3′ |
| | Reverse | 5′-GGGAGTGTTGATGTCAGTGTG-3′ |
| *Il-10* | Forward | 5′-GCCCAGAAATCAAGGAGCAT-3′ |
| | Reverse | 5′-TGTAGACACCTTGGTCTTGGAG-3′ |
| *Il13* | Forward | 5′-CCTCTGACCCTTAAGGAGCTTAT-3′ |
| | Reverse | 5′-CGTTGCACAGGGGAGTCT-3′ |
| *Tgfβ1* | Forward | 5′-CCTGAGTGGCTGTCTTTTGA-3′ |
| | Reverse | 5′-CGTGGAGTTTGTTATCTTTGCTG-3′ |
| *18S* | Forward | 5′-GTGATCCCTGAGAAGTTCCAG-3′ |
| | Reverse | 5′-TCGATGTCTGCTTTCCTCAAC-3′ |
| *Camp* | Forward | 5′-CAAGGGGACGAGGATCCAG-3′ |
| | Reverse | 5′-ATCTTCTCCCCACCTTTGCG-3′ |
| *Defb4* | Forward | 5′-CTCCTGGTGCTGCTGTCTCC-3′ |
| | Reverse | 5′-GCCACAATTGCCAATCTGTCG-3′ |
| *Lcn2* | Forward | 5′-GCCCAGGACTCAACTCAGAAC-3′ |
| | Reverse | 5′-ATCCAGTAGCGACAGCCCTG-3′ |
| *Cxcr6* | Forward | 5′-GTGAGCACACTTCACTCTGG-3′ |
| | Reverse | 5′-CCAGGTACACACAGGGCAAA-3′ |
| *Cxcl16* | Forward | 5′-AGCGCAAAGAGTGTGGAACT-3′ |
| | Reverse | 5′-GGTTGGGTGTGCTCTTTGTT-3′ |
| *Il-15* | Forward | 5′-CATCCATCTCGTGCTACTTGTGTT-3′ |
| | Reverse | 5′-CATCTATCCAGTTGGCCTCTGTTT-3′ |
| *Tslpr* | Forward | 5′-GAGCCTGGAGTTCCGTTATG-3′ |
| | Reverse | 5′-CAGTCACGTCCCCGTCTG-3′ |
| *Il-7ra* | Forward | 5′-GCAAGGGGTGAAAGCAACTG-3′ |
| | Reverse | 5′-CCCATCCTCCTTGATTCTTGG-3′ |
| *Ccr7* | Forward | 5′-GGAAAAACGTGCTGGTGGTG-3′ |
| | Reverse | 5′-CATGAGAGGCAGGAACCAGG-3′ |

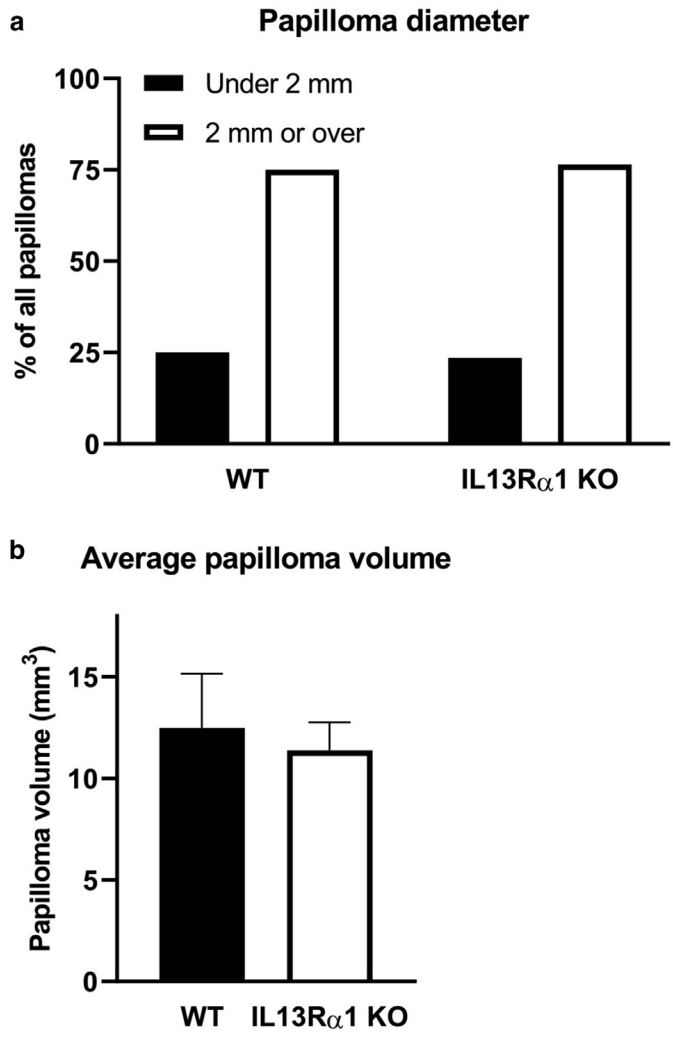


**Figure S1. The deletion of *Il-13rα1* has no effect on skin tumor size distribution.** (**A**) The percentage of papillomas under 2 mm (solid bars) and 2 mm or over (open bars). The data was analyzed with chi-square test, n = 10 for both groups. (**B**) The average size of papillomas per one mouse. The volume was estimated using the papilloma diameters and an assumption of spherical shape. The data was analyzed with Student's t-test, n = 10 for both groups.

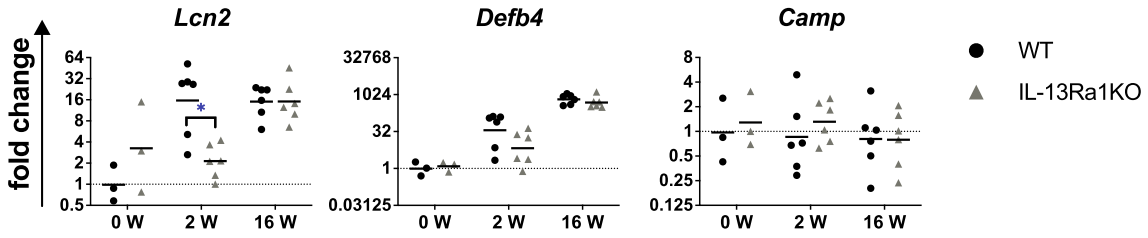


**Figure S2. Expression of antimicrobial peptides in mouse skin after DMBA/TPA treatment.** *Il-13rα1*-KO mice and their wild type (WT) counterparts were subjected to DMBA/TPA induced skin carcinogenesis as described in methods. At 0 (untreated), 2 or 16 weeks after DMBA/TPA treatment RNA from skin biopsies was extracted and qPCR analysis for *Camp, Lcn2* and *Defb4* was performed. ddCT method was used in analysis and graphs represent fold changes ($2^{-\Delta\Delta Ct}$ method) in (2-fold) logarithmic Y axis. In graphs, each symbol represents an individual mouse (mean of three technical replicates per mouse), lines indicate the geometric mean. The data was analyzed with Mann Whitney U test, *$p < 0.05$, **$p < 0.01$, ***$p < 0.001$. Mouse number used: 3-6 per group as indicated.

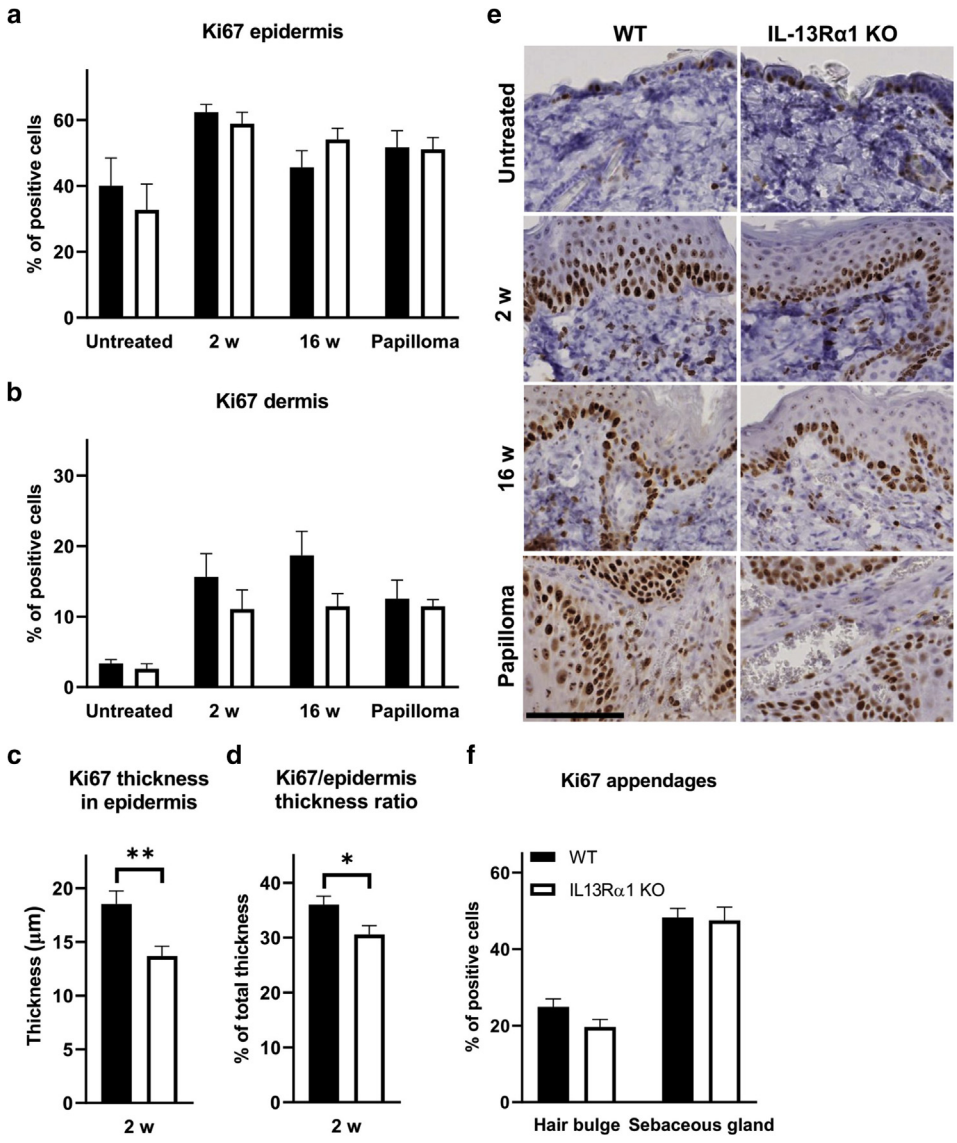


**Figure S3. Proliferating cells in the skin of DMBA/TPA treated mice.** *Il-13rα1* deficient mice and their wild type counterparts were subjected to DMBA/TPA induced skin carcinogenesis. (**A**) The percentage of the Ki67-positive cells in the epidermis of wild type (solid bars) and knock-out mice (open bars) before the DMBA/TPA treatment (Untreated), after two weeks of the treatment (2 w) and the normal skin (16 w) and papillomas (Papilloma) at the end of the experiment. The data was analyzed with Student's t-test, n = 10 for all groups. (**B**) The percentage of the Ki67-positive cells in the dermis of wild type (solid bars) and knock-out mice (open bars) before the DMBA/TPA treatment (Untreated), after two weeks of the treatment (2 w) and the normal skin (16 w) and papillomas (Papilloma) at the end of the experiment. The data was analyzed with Student's t-test, n = 10 for all groups. (**C**) Absolute thickness of the Ki67-positive cell layers in the epidermis of wild type (solid bars) and knock-out mice (open bars) two weeks after the DMBA/TPA treatment (2 w). The data was analyzed with Student's t-test, n= 10 for all groups, $^{**}p < 0.01$. (**D**) Thickness of the Ki67-positive cell layers in ratio to the thickness of the whole epidermis of wild type (solid bars) and knock-out mice (open bars) two weeks after the DMBA/TPA treatment (2 w). The data was analyzed with Student's t-test, n= 10 for all groups, $^{*}p < 0.05$. (**E**) Representative histologic images of the Ki67-stainings before the DMBA/TPA treatment (Untreated), after two week of the treatment (2 w) and the normal skin (16 w) and papillomas (Papilloma) at the end of the experiment. Stained with Ki67 antibody and hematoxylin, scale bar 100 µm. (**F**) The percentage of Ki67-positive cells in the hair bulges and sebaceous glands of wild type (solid bars) and knock-out mice (open bars) after two weeks of the DMBA/TPA treatment. The data was analyzed with chi-square test, n = 10 per group.

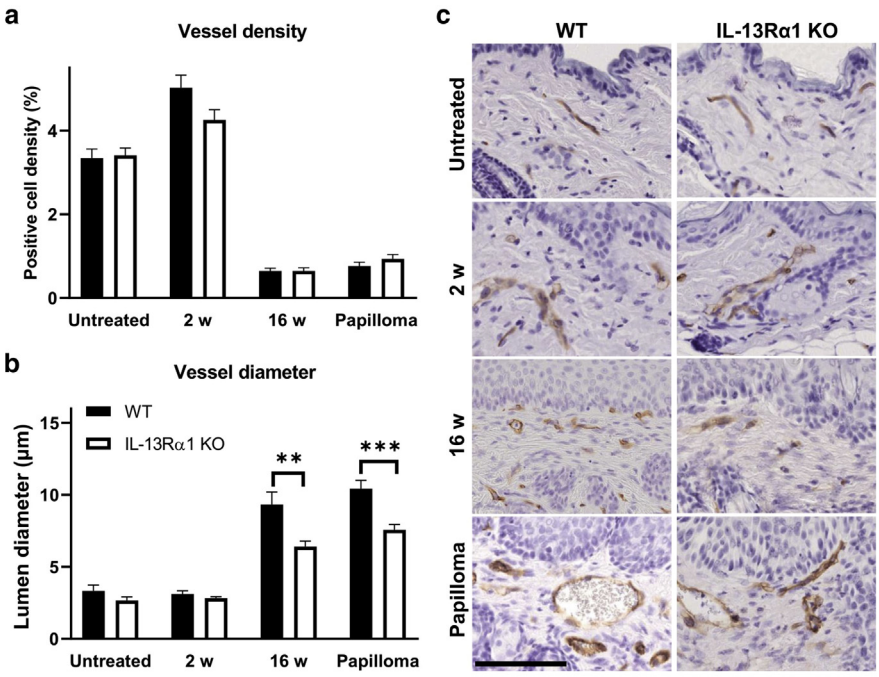


**Figure S4. The vessel density and width in the skin of DMBA/TPA treated mice.** *Il-13rα1* deficient mice and their wild type counterparts were subjected to DMBA/TPA induced skin carcinogenesis. (**A**) The percentage of the CD31-positive area in the dermis of wild type (solid bars) and knock-out mice (open bars) before the DMBA/TPA treatment (Untreated), after two weeks of the treatment (2 w) and the normal skin (16 w) and papillomas (Papilloma) at the end of the experiment. The data was analyzed with Student's t-test, n = 10 for all groups. (**B**) The width of the CD31-stained vessel lumens in the dermis of wild type (solid bars) and knock-out mice (open bars) before the DMBA/TPA treatment (Untreated), after two weeks of the treatment (2 w) and the normal skin (16 w) and papillomas (Papilloma) at the end of the experiment. The data was analyzed with Student's t-test, **p<0.01, ***p<0.001, n = 10 for all groups. (**C**) Representative histologic images of the CD31-stainings before the DMBA/TPA treatment (Untreated), after two weeks of the treatment (2 w) and the normal skin (16 w) and papillomas (Papilloma) at the end of the experiment. Stained with CD31 antibody and hematoxylin, scale bar 100 µm.

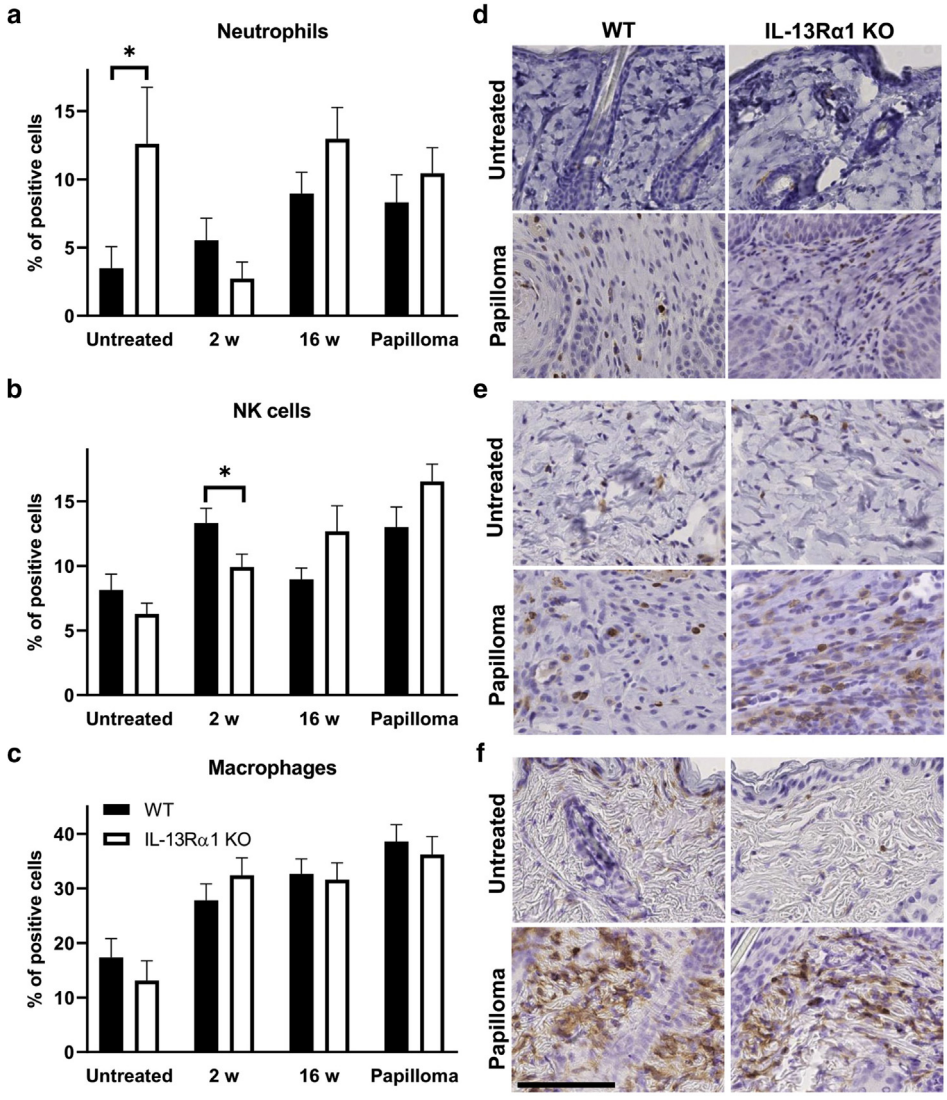


**Figure S5. Neutrophils, natural killer cells and macrophages in the skin of DMBA/TPA treated mice.** *Il-13rα1* deficient mice and their wild type counterparts were subjected to DMBA/TPA induced skin carcinogenesis. (**A**) The percentage of the neutrophil elastase-positive cells in the dermis of wild type (solid bars) and knock-out mice (open bars) before the DMBA/TPA treatment (Untreated), after two weeks of the treatment (2 w) and the normal skin (16 w) and papillomas (Papilloma) at the end of the experiment. The data was analyzed with Student's t-test, *$p<0.05$, n = 10 for all groups. (**B**) The percentage of the Cd49b-positive cells in the dermis of wild type (solid bars) and knock-out mice (open bars) before the DMBA/TPA treatment (Untreated), after two weeks of the treatment (2 w) and the normal skin (16 w) and papillomas (Papilloma) at the end of the experiment. The data was analyzed with Student's t-test, *$p<0.05$, n = 10 for all groups. (**C**) The percentage of the F4/80-positive cells in the dermis of wild type (solid bars) and knock-out mice (open bars) before the DMBA/TPA treatment (Untreated), after two weeks of the treatment (2 w) and the normal skin (16 w) and papillomas (Papilloma) at the end of the experiment. The data was analyzed with Student's t-test, n = 10 for all groups. (**D**) Representative histologic images of the neutrophil elastase-stainings before the DMBA/TPA treatment (Untreated) and the papillomas (Papilloma) at the end of the experiment. Stained with neutrophil elastase antibody and hematoxylin, scale bar 100 μm. (**E**) Representative histologic images of the CD49b-stainings before the DMBA/TPA treatment (Untreated) and the papillomas (Papilloma) at the end of the experiment. Stained with CD49b antibody and hematoxylin, scale bar 100 μm. (**F**) Representative histologic images of the F4/80-stainings before the DMBA/TPA treatment (Untreated) and the papillomas (Papilloma) at the end of the experiment. Stained with F4/80 antibody and hematoxylin, scale bar 100 μm.

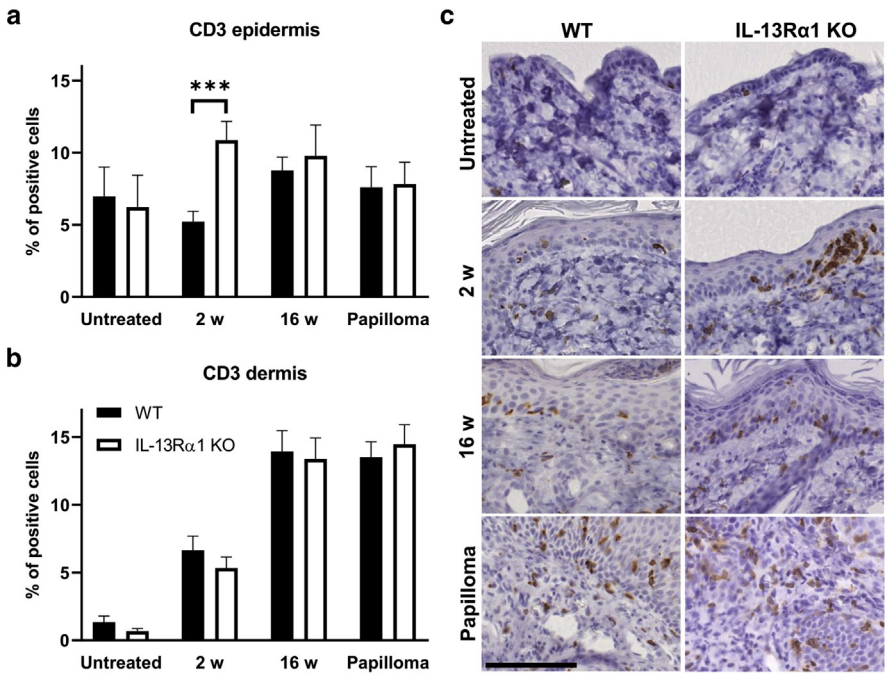


**Figure S6. T cells in the skin of DMBA/TPA treated mice.** *Il-13rα1* deficient mice and their wild type counterparts were subjected to DMBA/TPA induced skin carcinogenesis. (**A**) The percentage of the CD3-positive cells in the epidermis of wild type (solid bars) and knock-out mice (open bars) before the DMBA/TPA treatment (Untreated), after two weeks of the treatment (2 w) and the normal skin (16 w) and papillomas (Papilloma) at the end of the experiment. The data was analyzed with Student's t-test, ***$p<0.001$, $n = 10$ for all groups. (**B**) The percentage of the CD3-positive cells in the dermis of wild type (solid bars) and knock-out mice (open bars) before the DMBA/TPA treatment (Untreated), after two weeks of the treatment (2 w) and the normal skin (16 w) and papillomas (Papilloma) at the end of the experiment. The data was analyzed with Student's t-test, $n = 10$ for all groups. (**C**) Representative histologic images of the CD3-stainings before the DMBA/TPA treatment (Untreated), after two weeks of the treatment (2 w) and the normal skin (16 w) and papillomas (Papilloma) at the end of the experiment. Stained with CD3 antibody and hematoxylin, scale bar 100 μm.

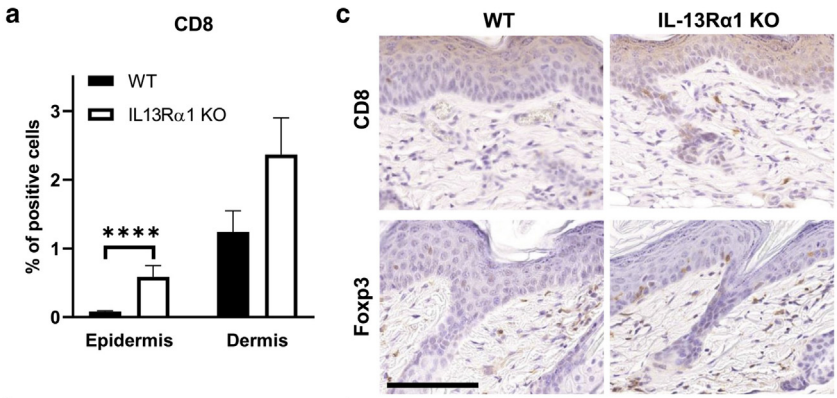


d

| Hair bulges | | Positive | Negative |
|---|---|---|---|
| CD3 | WT | 3.33% | 96.67% |
| | IL13Rα1 KO | 2.53% | 97.47% |
| CD8 | WT | 7.22% | 92.78% |
| | IL13Rα1 KO | 9.00% | 91.00% |
| Foxp3 | WT | 90.00 % | 10.00 % * |
| | IL13Rα1 KO | 96.50% | 3.50 % * |

**Figure S7. T cell subtypes in the skin after two weeks of DMBA-treatment.** *Il-13rα1* deficient mice and their wild type counterparts were subjected to DMBA/TPA-induced skin carcinogenesis. (**A**) The percentage of the CD8-positive cells in the epidermis and dermis of wild type (solid bars) and knock-out mice (open bars) after two weeks of the DMBA/TPA treatment. The data was analyzed with Student's t-test, ****$p<0.0001$, n = 8 for WT and n = 10 for KO. (**B**) The percentage of the FOXP3-positive cells in the epidermis and dermis of wild type (solid bars) and knock-out mice (open bars) after two weeks of the DMBA/TPA treatment. The data was analyzed with Student's t-test, n = 10 for dermis and n = 9 for epidermis. **(C)** Representative histologic images of the CD8 and FOXP3 stainings before the DMBA/TPA treatment (Untreated) or after two weeks of the treatment. Stained with CD8 or FOXP3 antibody and hematoxylin, scale bar 50 μm. **(D)** The percentage of CD3, CD8, and FOXP3-positive and negative hair bulges out of all hair bulges of wild type and knock-out mice after two weeks of the DMBA/TPA treatment. The data was analyzed with chi-square test, *$p<0.05$, n = 10 for CD8 KO and FOXP3 KO, n = 9 for CD3 WT, CD8 WT and FOXP3 WT, n = 8 for CD3 KO.

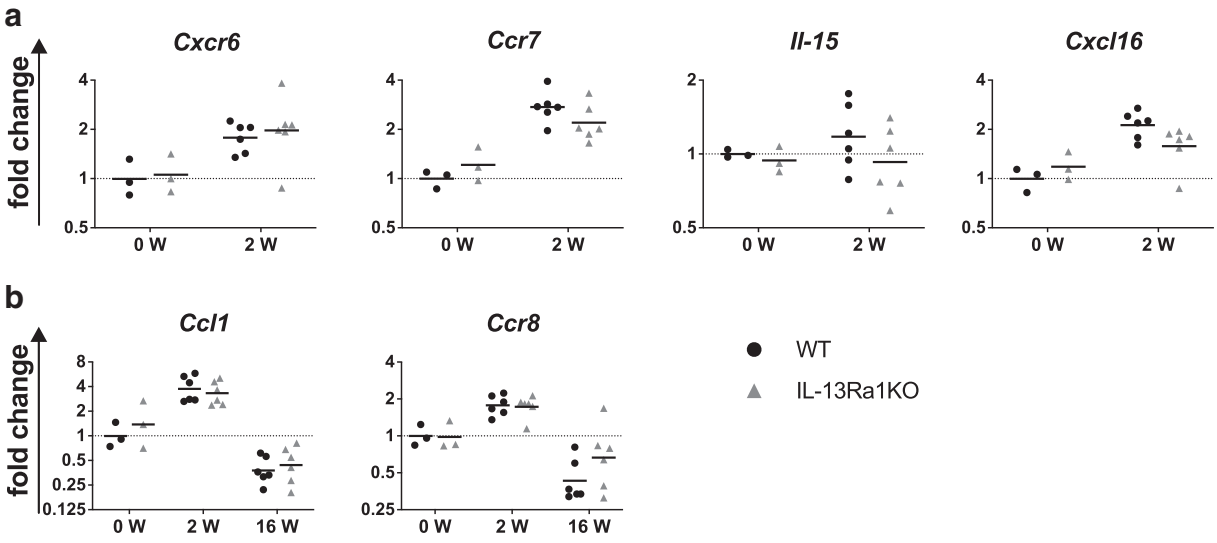


**Figure S8. qPCR analysis of gene expression of CD8 cell and Treg network related genes in mouse skin after DMBA/TPA treatment.** *Il-13rα1*-KO mice and their wild type (WT) counterparts were subjected to DMBA/TPA induced skin carcinogenesis as described in methods. At 0 (untreated), 2 or 16 weeks after DMBA/TPA treatment RNA from skin biopsies was extracted and qPCR analysis for (**A**) *Cxcr6, Cxcl16, Il-15* and *Ccr7* for CD8 T cell recruitment or (**B**) *Ccr8* and *Ccl1* for T regs was performed. ddCT method was used in analysis and graphs represent fold changes ($2^{-\Delta\Delta Ct}$ method) in (2-fold) logarithmic Y axis. In graphs, each symbol represents an individual mouse (mean of three technical replicates per mouse), lines indicate the geometric mean. The data was analyzed with Mann Whitney U test, *$p < 0.05$, **$p < 0.01$, ***$p < 0.001$. Mouse number used: 3-6 per group as indicated.

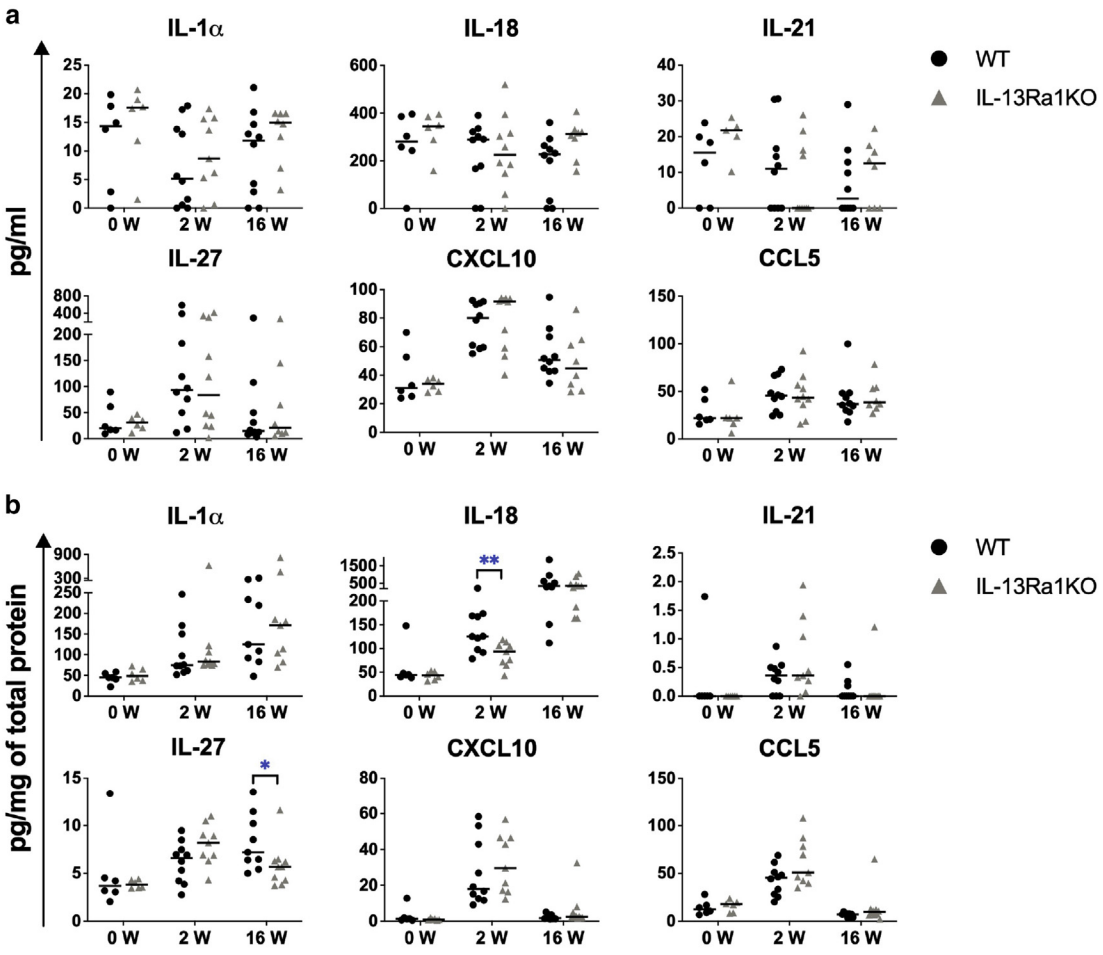


**Figure S9. Systemic and local cytokine and chemokine production in serum and skin during papilloma formation.** *Il-13rα1*-KO mice and their wild type (WT) counterparts were subjected to DMBA/TPA induced skin carcinogenesis as described in methods. At 0 (untreated), 2 and 16 weeks after DMBA/TPA treatment, animals were sacrificed, and serum and skin samples were collected. Skin samples were homogenized as described in methods. Cytokine levels were determined from serum (**A**) and from skin homogenate lysates (**B**). Skin data was normalized to total protein concentration in each sample. In graphs, each symbol represents an individual mouse, lines indicate the median. The data was analyzed with Mann Whitney U test, *$p < 0.05$, **$p < 0.01$, ***$p < 0.001$. Mouse number used: in serum: untreated: n=6 per strain, at 2 W: n=10 per strain and at 16 W: n=10 for WT and n=8 for KO strains. Mouse number used: in skin: untreated: n=6 per strain, at 2 W: n=10 for WT and n=9 for KO strains, and at 16 W: n=9 for WT and n=10 for KO strains.

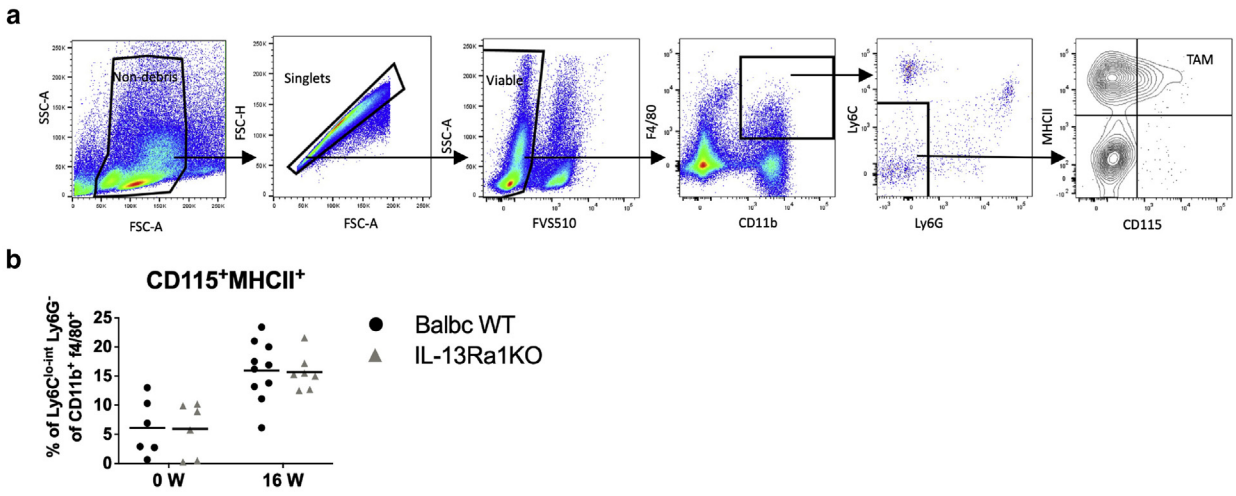


**Figure S10. Number of tumor associated macrophages (TAMs) in spleen during papilloma formation.** *Il-13rα1*-KO mice and their wild type (WT) counterparts were subjected to DMBA/TPA induced skin carcinogenesis as described in methods. At 0 (untreated) and 16 weeks after DMBA/TPA treatment, animals were sacrificed, and spleens were isolated and stained for flow cytometry as described in methods. TAMs were defined as $CD11b^{+}$ $f4/80^{+}$ $Ly6C^{lo/int}Ly6G^{-}$ $CD115^{+}$ MHC $II^{+}$. (**A**) Gating strategy and representative figure of TAMs in spleen. (**B**) Percentages of these cells in spleen. In graphs, each symbol represents an individual mouse, lines indicate the mean. The data was analyzed with Student's t-test, *$p < 0.05$, **$p < 0.01$, ***$p < 0.001$. Mouse number used: untreated: n=6 per strain and at 16 W: n=10 for WT and n=7 for KO strains.

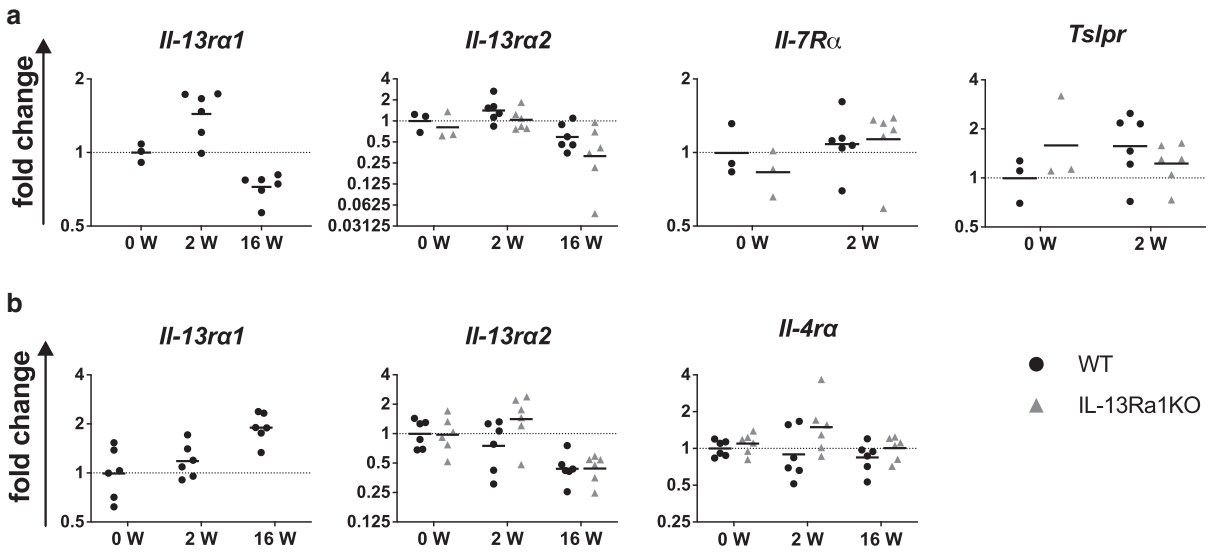


**Figure S11. qPCR analysis of gene expression of receptor chains in skin and spleen during papilloma formation.** *Il-13rα1*-KO mice and their wild type (WT) counterparts were subjected to DMBA/TPA induced skin carcinogenesis as described in methods. At 0 (untreated), 2 or 16 weeks after DMBA/TPA treatment, animals were sacrificed, and spleen and skin were collected and processed as described in methods. qPCR analysis was performed from skin (**A**) and from serum (**B**) samples. *IL-13Rα1* was undetermined in KO mice in skin and spleen samples. ddCT method was used in analysis and graphs represent fold changes ($2^{-\Delta\Delta Ct}$ method) in (2-fold) logarithmic Y axis. In graphs, each symbol represents an individual mouse (mean of three technical replicates per mouse), lines indicate the geometric mean. The data was analyzed with Mann Whitney U test, *p < 0.05, **p < 0.01, ***p < 0.001. Mouse number used: 3-6 per group as indicated.

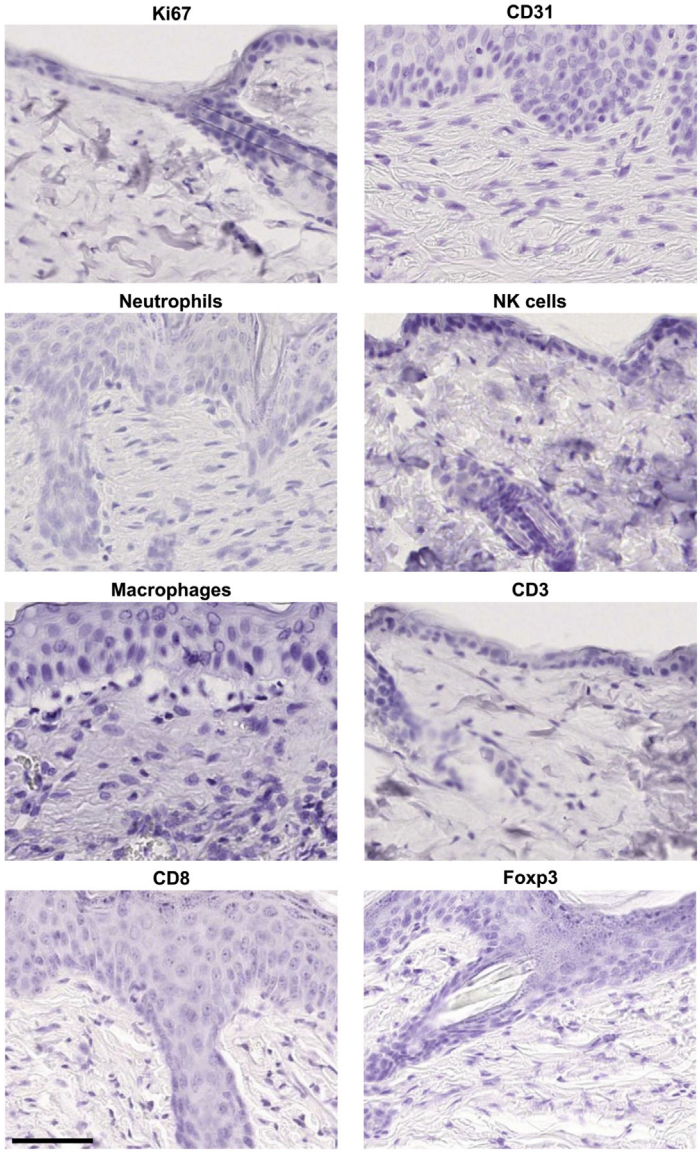


**Figure S12. The negative controls of the antibodies used.** *Il-13rα1* deficient mice and their wild type counterparts were subjected to DMBA/TPA incudes skin carcinogenesis. Representative images of the negative control stainings. Scale bar 200 μm.